HHS Public Access

Author manuscript

Curr Biol. Author manuscript; available in PMC 2023 August 08.

Published in final edited form as:

Curr Biol. 2022 August 08; 32(15): 3350–3364.e6. doi:10.1016/j.cub.2022.06.040.

Ets21C sustains a pro-regenerative transcriptional program in blastema cells of *Drosophila* imaginal discs

Melanie I. Worley[1,4,*,†], **Nicholas J. Everetts**[1,2,*], **Riku Yasutomi**[1], **Rebecca J. Chang**[1], **Shrey Saretha**[1], **Nir Yosef**[2,3,†], **Iswar K. Hariharan**[1,5,6,†]

[1]Department of Molecular and Cell Biology, University of California, Berkeley

[2]Department of Electrical Engineering and Computer Science, Center for Computational Biology, University of California, Berkeley

[3]Chan Zuckerberg Biohub Investigator, San Francisco, CA, USA

[4]Twitter: @D_Melaniegaster

[5]Twitter: @HariharanLab

[6]Lead contact

Summary

An important unanswered question in regenerative biology is to what extent regeneration is accomplished by the re-activation of gene regulatory networks used during development versus the activation of regeneration-specific transcriptional programs. Following damage, *Drosophila* imaginal discs, the larval precursors of adult structures, can regenerate missing portions by localized proliferation of damage-adjacent tissue. Using single-cell transcriptomics in regenerating wing discs, we have obtained a comprehensive view of the transcriptome of regenerating discs and identified two regeneration-specific cell populations within the blastema, Blastema1 and Blastema2. Collectively, these cells upregulate multiple genes encoding secreted proteins that promote regeneration including *Pvf1*, *upd3*, *asperous, Mmp1*, and the maturation delaying factor *Ilp8*. Expression of the transcription factor Ets21C is restricted to this regenerative secretory zone; it is not expressed in undamaged discs. *Ets21C* expression is activated by the JNK/AP-1 pathway and it can function in a type 1 coherent feed-forward loop with AP-1 to sustain expression of downstream genes. Without *Ets21C* function, the blastema cells fail to maintain the expression of a number of genes, which leads to premature differentiation and severely compromised regeneration. As *Ets21C* is dispensable for normal development, these observations indicate that

†Corresponding authors: mworley@berkeley.edu (M.I.W.), niryosef@berkeley.edu (N.Y.), ikh@berkeley.edu (I.K.H.).
*These authors contributed equally to this work.

Author Contributions: M.W. and N.E. contributed equally. Project conceived and designed, M.W., N.E., N.Y., and I.H. Experimental design, M.W., N.E., R.Y., N.Y., and I.H. Experiments conducted and analyzed by M.W., N.E., R.Y., R.C., and S.S. Computational analysis performed by N.E. and M.W. Writing- original draft, M.W. and I.H. Writing- revision, M.W., N.E., and I.H. Review & editing, M.W., N.E., R. Y., R.C., N.Y., and I.H. Funding acquisition, N.Y. and I.H.

Declaration of Interest: The authors declare no competing interests.

Ets21C orchestrates a regeneration-specific gene regulatory network. We have also identified cells resembling both Blastema1 and Blastema2 in *scribble* tumorous discs. They express the *Ets21C*-dependent gene regulatory network and eliminating *Ets21C* function reduces tumorous growth. Thus, mechanisms that function during regeneration can be co-opted by tumors to promote aberrant growth.

eTOC blurb

Regeneration requires cell-specific transcriptional responses. Worley, Everetts, *et al.* investigate the gene regulatory networks that are activated during regeneration and find that the transcription factor Ets21C is critical for effective regeneration by sustaining a pro-regenerative transcriptional program in a subpopulation of blastema cells.

Graphical Abstract

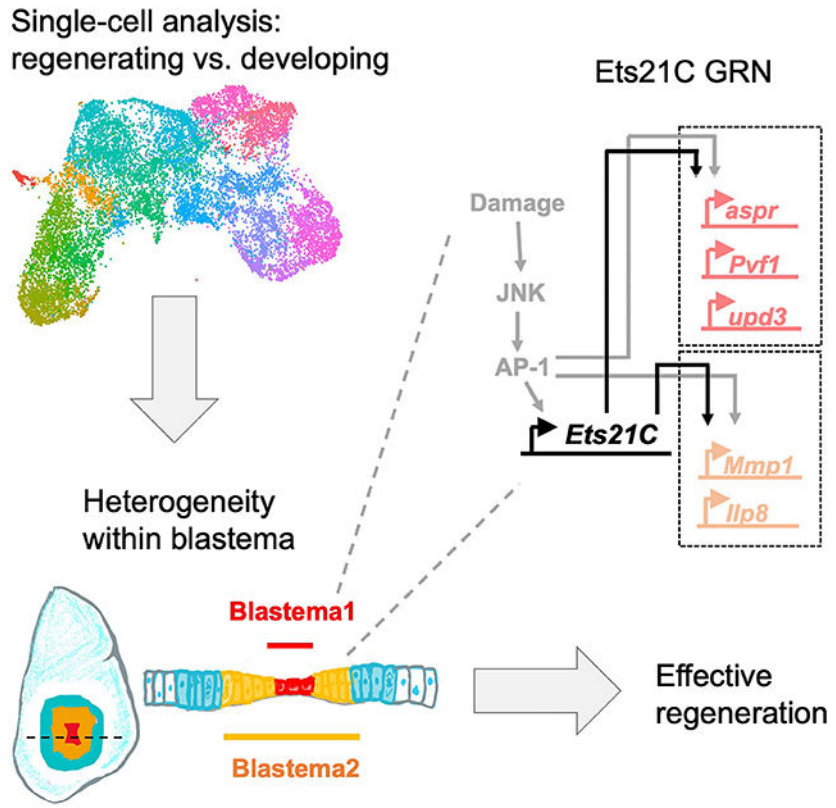

Introduction

Regeneration is the process by which tissue that has been damaged or lost is replaced by tissue that is functionally equivalent. Dramatic examples of regeneration include whole-body regeneration in the cnidarian *Hydra* [1] and in flatworms [2]. Among vertebrates, tadpoles can regenerate their tails [3] and urodele amphibians such as salamanders can regenerate severed limbs [4]. During appendage regeneration, the tissue that has been lost is replaced by the proliferation and re-specification of more proximally fated cells. Typically, there is

a localized zone of proliferation of relatively undifferentiated cells known as a regeneration blastema [5]. Cells generated by the blastema eventually adopt differentiated fates. The genetic regulation of many aspects of regenerative growth including blastema formation and cell fate re-specification are not well understood. Many mysteries remain about how individual cells coordinate during regeneration to effectively replace missing or damaged tissue. A key unanswered question is whether regeneration is mainly accomplished by the reactivation of developmental gene regulatory networks (GRNs) or, alternatively, by the activation of GRNs that primarily function during regeneration.

While appendage regeneration has been primarily investigated using approaches derived from experimental embryology (e.g. tissue transplantation), the organisms that have been studied are not especially amenable to genetic manipulation. In contrast, *Drosophila melanogaster* is especially suited to using genetic approaches to deconstruct complex biological processes such as embryonic patterning and growth regulation. The imaginal discs of *Drosophila*, the larval precursors of adult tissue, are capable of regeneration following damage if they are transplanted into other larvae or into the abdomens of adult flies [6]. More recently, genetic tissue ablation systems have been developed that enable damage of a specific region of imaginal discs such that regeneration occurs *in situ* [7,8]. Imaginal disc regeneration is accomplished through formation of a blastema, similar to that described in vertebrates and characterized by highly-localized proliferation [9]. Some studies have been able to identify genes expressed in the blastema by physically separating the blastema from the rest of the disc [10] or by separating the cells of the blastema by flow cytometry [11]. However, since the blastema comprises a small portion of the imaginal disc, it has been difficult to characterize its properties in detail.

Single-cell RNA sequencing (scRNAseq) offers a way to obtain a detailed view of the unique cellular types and transcriptional response during regeneration. Studies of regenerating tissues have provided evidence for cellular states and gene expression patterns that do not occur during normal development and are therefore potentially regeneration specific (for example [12,13]). To date, there is little evidence for GRNs that are functionally needed for regeneration but not for normal development (reviewed by [14]). Here, we use scRNAseq to characterize unappreciated cellular heterogeneity within the blastema of regenerating discs. In particular, we identify these cells as secreting multiple pro-regenerative factors under the control of the transcription factor Ets21C, and find that Ets21C is essential for regenerative growth yet dispensable for developmental growth. We also identify a subpopulation of blastema-like cells during tumorous overgrowth, indicating parallels between regeneration and oncogenesis.

Results

To identify transcriptional programs that function during regeneration, we examined the regeneration of *Drosophila* larval wing imaginal discs, the epithelial tissues that differentiate into the adult wing blades and dorsal thorax. Imaginal discs are capable of regenerating after damage through the formation of a blastema, defined by localized proliferation and increased cellular plasticity [9] (reviewed by [15,16]). To search for regeneration-specific GRNs, we compared regenerating and developing wing discs using single-cell transcriptomics.

Tissue damage was induced by temporarily expressing the pro-apoptotic TNF ortholog *eiger* within the wing pouch [7] (Figure S1A), the cells that give rise to the most distal-fated tissues of the wing disc, the wing blade. Subsequent regeneration occurs by localized cell proliferation and cell-fate re-specification, likely from more proximal-fated cells that normally generate the hinge [7,17], the structure that attaches the wing blade to the thorax. We collected wing discs after 24 hours of regeneration, approximately one-third of the way through the regenerative process, and sequenced a total of 14,320 cells from two biological replicates, with an average of >3,000 genes detected per cell. Three major cell types were identified: epithelial cells, myoblasts, and hemocytes (Figure S1B–F). Since imaginal disc regeneration is driven by epithelial cell proliferation [7,9,18], we focused further analysis on these cells.

To identify potential regeneration-specific GRNs, we harmonized the epithelial cell data from regenerating discs with our previously collected data from undamaged discs [19] using scVI [20,21] (see Materials and Methods) (Figure 1A, B). We assigned cell clusters to specific subregions of the wing disc epithelium based on the expression of known marker genes [19,22,23,24] (Figure 1B, C). As expected, cell clusters with pouch identity were underrepresented in the regenerating sample, as this portion of the tissue was ablated (Figure S1G, H). We observed two clusters, denoted Blastema1 and Blastema2, that were almost exclusively composed of cells from the regenerating sample (181/186 and 519/564 cells, respectively) (Figure 1C; Figure S1H). Thus, we have identified cell states that are present in regenerating discs but not in undamaged discs. Within these two regeneration-specific clusters, we observed the upregulation of genes known to be induced around the site of damage, including *wingless* (*wg*) and *Wnt6* [25,26], *Matrix metalloproteinase 1* (*Mmp1*) [27], *Insulin-like peptide 8* (*Ilp8*) [10,28], and *asperous (aspr*) [29] (Figure 1C–F).

Both Blastema1 and Blastema2 clusters express *Ilp8*, which is strongly upregulated around the site of damage in the regenerating disc (Figure 1D, G, H). However, Blastema2 showed a higher expression of hinge-identity markers, such as *Zn finger homeodomain 2* (*zfh2*), than Blastema1 (Figure 1C). The increased expression levels of hinge-identity markers within Blastema2 suggests that these cells might occupy an outer position compared to Blastema1 cells. Indeed, in regenerating tissue, we observed higher Zfh2 expression in the outer ring of *Ilp8*-expressing cells (Figure 1H) albeit at lower levels than the surrounding hinge cells. In contrast, Blastema1 cells expressed higher levels of the unpaired-family genes (*upd1, upd2, upd3*), *aspr*, and *PDGF- and VEGF-related factor 1* (*Pvf1*) (Figure 1C, E–F). The Upd ligands activate the JAK/STAT pathway, which is important for cellular plasticity and regeneration [28,30–32]. The gene *aspr* encodes a secreted protein with multiple EGF-repeats important for regeneration [29]. Pvf1 binds to its receptor Pvr and the resulting signaling is known to contribute to wound healing [33], and homologs are involved in regeneration in other systems [34,35]. To detect the location of multiple transcripts simultaneously within regenerating tissue, we performed *in situ* RNA hybridization using the hybridization chain reaction (HCR) technique [36] (see Materials and Methods). We determined that *Pvf1*, *upd3*, and *Ilp8* were all expressed at the center of the blastema (Figure 1I, J), which is surrounded by cells that express *Ilp8* but not *Pvf1* or *upd3*. Thus, the Blastema1 cells are located at the center of the blastema and are surrounded by Blastema2 cells; cells in both regions secrete

ligands, some of which are known to promote regeneration, and are likely acting on the surrounding tissue.

To determine the temporal dynamics of these two blastema cell states, we used HCR probes for genes that mark these two populations of cells (*Ilp8* and *aspr*) (Figure 2A–D). Based on these marker genes, we observed that the *aspr*-expressing cells initially represent a larger fraction of the *Ilp8*-expressing cells. The area of *aspr* expression decreases progressively from the end of the ablation period (R0) until being largely absent by 48 hours of regeneration (R48). In contrast, *Ilp8* is still being transcribed at R48 (Figure 2C). The progressive decrease in the number of Blastema1 cells could indicate that they represent a transient population that orchestrates regeneration and is eventually eliminated. Alternatively, Blastema1 cells could change their properties and eventually contribute to the regenerate. To distinguish between these possibilities, we marked cells at the center of the regenerating tissue by utilizing a UAS-driven FLP to mark cells that express *rn-GAL4.* In contrast to previous work [7,17,32,37], we used a destabilized FLP to preferentially mark those cells that expressed high levels of *rn-Gal4* by inducing the removal of a stop FLP-out cassette (*Ubi-FRT-stop-FRT-GFP).* This permanently marked cells that expressed *rn-GAL4* during the ablation period (when the $GAL80^{ts}$ repressor is inactive). We found that this method specifically labeled the cells at the center of the blastema which, at early time points, are in the Blastema1-state. We found that these cells were able to contribute to the regenerating tissue at R48 when the Blastema1 state is mostly absent. This indicates that at least some of the Blastema1 cells remain in the tissue and contribute to the regenerate.

We next asked if non-blastema cells could be directly recruited to take on a Blastema2-cellular state. To address this question, we took advantage of the temporal dynamics of RNA and protein expression to determine if additional *Ilp8*-expressing cells were being recruited and to visualize the location of these cells. We expected that cells beginning to express *Ilp8* would have detectable RNA but no fluorescent GFP (from *Ilp8-GFP*). We observed that at an early time point in regeneration, cells surrounding the blastema showed higher levels of *Ilp8* RNA than GFP (Figure 2E). This indicates that cells on the periphery are newly recruited blastema cells. By 24 h of regeneration (R24), *Ilp8 RNA* and GFP fluorescence mostly overlapped (Figure 2F), indicating that the population of cells expressing Ilp8 have reached a steady state. By R48, *Ilp8* RNA expression was only detected in the center of the GFP-expressing region (Figure 2G). This dynamic change can be observed by quantification of expression levels at distances from the center of the blastema (Figure 2H). The early expansion of *Ilp8* expression indicates that non-blastema cells can be recruited to a blastema state, while the subsequent contraction of the domain of *Ilp8* RNA expression indicates that blastema cells can become non-blastema cells. Thus, the blastema-state is a transient cellular state and not an immutable property of cells.

Where do the blastema cells originally come from? We used developmental-patterning gene signatures to determine that the cells within the regenerative secretory zone (Blastema1 and 2) were in an intermediate state between hinge and pouch identities (Figure 2I; Figure S2A–C). This finding suggested that these cells were derived from the surrounding inner-hinge region and were in the process of acquiring more distal pouch fates. To investigate this process, we examined the location of proliferating cells and found high levels of

EdU incorporation surrounding the regenerative secretory zone (Figure 2J); the absence of proliferation in the most central region of the regenerating pouch was previously noted [37]. As regeneration proceeded, the EdU incorporation extended more centrally to occur within the regenerative secretory zone (Figure 2K).

To determine if these proliferating cells are reprogrammed during regeneration to replace the ablated pouch, we marked cells that expressed an inner-hinge enhancer (Figure 2L). In the absence of pouch ablation, these cells and their progeny remain confined to a ring around the pouch (Figure 2M). At an early time point during regeneration, cells at the center of the blastema are derived from cells that still express this enhancer as assessed by the perdurance of a stable RFP (Figure 2N). By permanently marking these cells with a lineage tracing tool, we observed that following regeneration, most of the regenerated pouch was derived from cells that once expressed this enhancer (Figure 2O). This indicates the cells from the hinge are re-programmed to take on blastema cell fates which form the majority of the regenerate. Our single-cell trajectory analysis suggests that cells transition through a Blastema2 cell state during reprogramming (Figure S2D–E). This is consistent with previous observations that hinge-cells can contribute to the pouch during regeneration [17,38]. Thus, the ablated pouch is regenerated by the proliferation and reprogramming of more proximally fated inner hinge cells, likely driven by the ligands secreted by the regenerative secretory zone (Figure 2P).

To search for a regulator of these regeneration-specific transcriptional changes, we analyzed our single-cell data for a transcription factors that were specifically expressed within the Blastema1 and 2 clusters. We found that *Ets at 21C* (*Ets21C*) was expressed during regeneration, primarily within the cells of the regenerative secretory zone, and not in cells from developing wing discs which were undamaged (Figure 3A–C). *Ets21C* was also upregulated after physical wounding of the wing disc (Figure 3D), implying that Ets21C is involved in a general regeneration response. *Ets21C* had previously been shown to be upregulated during disc regeneration by microarray analysis of RNA [28] and bulk sequencing of blastema-enriched cells [11]. Our single-cell data indicates that *Ets21C* expression is highly correlated with *Ilp8* and *Mmp1* expression during regeneration (Figure S3A).

To determine the function of *Ets21C*, we turned to mutant analysis. First, we observed that homozygous $Ets21C^{-/-}$ null mutants generate viable and fertile adults, as previously noted [39], whose wings were of normal size and shape (Figure 3E–G). These mutants, however, develop defects in adult intestinal epithelial cell replacement as they age [39], but do not exhibit any reduction in lifespan as a consequence except under conditions of oxidative stress [39,40]. To determine if *Ets21C* was important for cell proliferation or viability during development, we generated mosaic eyes composed of marked wild-type and $Ets21C^{-/-}$ mutant cells and observed that mutant cells effectively contributed to the adult tissue and did not display defects in cell proliferation (Figure 3H, I). Thus, *Ets21C* is dispensable for normal development and its absence does not impair cell proliferation or survival.

Next, we tested if *Ets21C* was important for imaginal disc regeneration. Following our genetic ablation assay, homozygous null $Ets21C^{-/-}$ mutants ($Ets21C^{\Delta 10/\Delta 10}$) showed a dramatic reduction in the extent of wing regeneration when compared to either $Ets21C^{+/-}$

heterozygotes or wild-type controls (Figure 3J, K). This effect was also observed with the null mutation in trans to two different chromosomal deletions that span the *Ets21C* locus (Figure 3J), indicating that the effect was indeed due to the loss of *Ets21C* function. Thus, Ets21C is required for effective imaginal disc regeneration.

Ets21C is part of the Ets-family of DNA-binding transcription factors that are broadly conserved in animals. The *Ets21C* mammalian orthologs are *Ets-related gene (ERG)* and *Friend Leukemia Integration 1 Transcription Factor (FLI1)*, both of which can act as oncogenes, most notably in the aggressive pediatric cancer Ewing's sarcoma [41]. In *Drosophila*, although *Ets21C* is not expressed in undamaged third instar wing discs, its expression is upregulated in tumorous imaginal discs [42,43] and it is involved in adult midgut homeostasis [39,44]. *Ets21C* is a downstream target of JNK/AP-1 signaling in these contexts [39,42,43]. Similarly, we found that even in undamaged discs, activation of the JNK pathway induces *Ets21C* expression (Figure S3B, C). The JNK/AP-1 pathway is known to be critical for regeneration [8,17,26,28,29,45,46]. *Ets21C* expression during regeneration is reduced when JNK signaling is blocked (Figure S3D, E), indicating that *Ets21C* is downstream of JNK/AP-1 signaling (Figure S3F). However, $Ets21C^{-/-}$ mutants do not exhibit other common phenotypes of loss of JNK/AP-1 signaling, such as the failures of dorsal closure during embryogenesis and imaginal-disc fusion during metamorphosis. Thus, *Ets21C* likely mediates only a subset of JNK functions, notably those that involve regeneration.

In order to characterize the genes that are regulated by Ets21C during regeneration, we profiled $Ets21C^{-/-}$ mutant regenerating tissues after 24 hours of regeneration with single-cell transcriptomics. We harmonized our data from developing and regenerating discs to directly compare similar cell types (Figure 4A). $Ets21C^{-/-}$ mutant regenerating tissues still contained Blastema1 and Blastema2 cells (Figure 4B), although the percentage of cells found in both blastema populations was reduced. Thus, *Ets21C* function is not required for the formation of the blastema *per se*. The Blastema1 cells from $Ets21C^{-/-}$ mutants had reduced expression of a number of genes, including genes that encode secreted molecules, including *Pvf1*; the unpaired family of genes *(upd1, 2, 3)*; and *aspr* (Figure 4C, D).

We investigated how these genes were expressed during the course of regeneration in wild type and $Ets21C^{-/-}$ mutant tissues. In wild-type regenerating discs, *upd3, Pvf1,* and *aspr* transcripts were detected within the center of the blastema at both the start (R0) and a midpoint during regeneration (R24) (Figure 4E–G). In contrast, regenerating $Ets21C^{-/-}$ mutant discs showed a substantial decrease of all three transcripts at both R0 and R24 timepoints (Figure 4E–G). Thus, *Ets21C* is required for sustained expression of *upd3, Pvf1*, and *aspr* within the inner regenerative secretory zone. In contrast, Wg expression during regeneration seems largely unaffected (Figure S4A–C).

We next examined if Ets21C regulates the expression of genes expressed in the outer regenerative secretory zone. Expression of both *Mmp1* and *Ilp8* was decreased within the $Ets21C^{-/-}$ mutant regenerating tissue, especially by 24 hours of regeneration (Figure 4H, I). To test whether *Ets21C* regulates *Ilp8* cell-autonomously, we generated mosaic discs containing $Ets21C^{-/-}$ mutant and wild-type cells prior to tissue damage. In these regenerating discs, $Ets21C^{-/-}$ mutant cells showed reduced *Ilp8-GFP* expression

as compared to wild-type cells (Figure S4D), indicating that Ets21C is required cell-autonomously to maintain *Ilp8* expression within the blastema. Together, this demonstrates that *Ets21C* is required to maintain the cellular states that constitute the inner and outer regenerative secretory zones.

What happens to regeneration when the regenerative secretory zone is not maintained? We observed changes in the pattern of cell proliferation during regeneration in *Ets21C* mutant discs (Figure 5A–F), indicating a prematurely reduced central non-proliferating zone. In wild-type regenerating discs, tissue-wide transcriptional changes indicate that the regenerating disc, including portions that have not been damaged, has a more juvenile transcriptional program than predicted by chronological age (Figure 5G; Figure S5A). In contrast, *Ets21C*$^{-/-}$ mutant cells exhibit a more advanced cellular maturity state (Figure 5G), indicating that *Ets21C* is required to maintain a more juvenile state during regeneration. Previous work suggested that the growth of other imaginal discs may pause during the process of wing-imaginal disc regeneration, based on the overall size of the imaginal discs [47]. Building on this, we quantified developmental progression within the eye disc by examining the advancement of the morphogenetic furrow and observed a distinct pause during regeneration (Figure S5B–D). In contrast, within *Ets21C*$^{-/-}$ larvae, this developmental delay of the morphogenetic furrow was not maintained (Figure S5E–F). Ilp8 is crucial for delaying pupariation [48,49], and more recently Upd3 has also been shown to contribute [50]. This developmental delay in pupariation is correlated with better regeneration outcomes [7,26,28,51–55]. Indeed, *Ets21C*$^{-/-}$ mutant animals ended the larval phase of development approximately 31h before regenerating controls (Figure S5G, H), which is likely the result of a decrease in both *upd3* and *Ilp8* levels as well as other signaling molecules.

From the single-cell data, we observed that more pouch cells were recovered from *Ets21C*$^{-/-}$ regenerating tissues (Figure 4B), suggesting that cells of the blastema had already started to become repatterned. In addition, the *Ets21C*$^{-/-}$ cells classified with blastema identity expressed increased levels of several genes that encode for pouch transcription factors, such as *rotund (rn)* and *nubbin (nub)* than the wild-type blastema (Figure 4C). This led us to hypothesize that a potential consequence of not maintaining the regenerative secretory zone was premature repatterning. Indeed, *Ets21C*$^{-/-}$ mutants expressed higher levels of Nub than wild-type discs by 24 hours of regeneration (Figure 5H–J). Thus, *Ets21C*$^{-/-}$ mutants have both local and systemic defects in their regenerative response that collectively contribute to the reduced regeneration.

Many Ets21C transcriptional targets in the blastema have also been described to be regulated by JNK/AP-1. While JNK/AP-1 signaling is especially active during the first half of regeneration (Figure 6A–E), *Ets21C* expression was maintained throughout regeneration (Figure 6F–J), suggesting that Ets21C functions to maintain a pro-regenerative state over the course of regeneration. We propose that Ets21C works downstream of AP-1 in a type-1 coherent feed-forward loop [56], where AP-1 induces the expression of *Ets21C*, and then together, these transcription factors induce the expression of downstream targets.

In support of this model, we found that the overexpression of either *Ets21C* or the AP-1 activator hep^{wt} was sufficient to induce the expression *Ilp8* even when the other branch was inactivated using RNAi (Figure 6K–O). In addition, the overexpression of *Ets21C* was also sufficient to induce the expression of *Pvf1* (Figure S6C–E). However, not all Ets21C-targets were induced in undamaged discs following *Ets21C* overexpression, as observed for *aspr* (Figure S6F–I), suggesting additional regulators are required for their activation. Overall, this model predicts that target genes could be induced when AP-1 becomes active and then be maintained by Ets21C as AP-1 activity fades (Figure 6P; Figure S6A). Consequently, in the absence of Ets21C function, target gene expression would fade more rapidly once AP-1 activity decreases.

While *Ets21C* function is required for regeneration and not necessary for normal development, it is known to be expressed in tumorous imaginal discs that have mutations that disrupt apicobasal polarity [42,43]. Moreover, in one study, reducing *Ets21C* function was shown to reduce the size of tumors caused by expressing oncogenic Ras and simultaneously reducing levels of the apicobasal polarity regulator *discs large* [43]. Recent single-cell studies of tumorous imaginal discs [22] caused by mutations in the apicobasal polarity regulator *scribble* (*scrib*) [57] have demonstrated considerable cellular heterogeneity [22,58]. By harmonizing our data with published single-cell RNAseq data derived from tumorous *scrib* discs [22] (Figure 7A, B), we identified cell clusters that have similar transcriptomes to the regenerative secretory zone (Blastema1 or Blastema2 cell clusters) (Figure 7C). Notably, these cell clusters together express *Ets21C* along with *upd3, Pvf1, Mmp1*, and *Ilp8* (Figure 7D, E) and are more prevalent at earlier stages of disc overgrowth (Figure 7F). Thus, while most cells in the disc have defects in apicobasal polarity, only a small subset of cells appear to activate this pro-regenerative GRN featuring *Ets21C*. Consistent with the hypothesis that blastema-like cells could be critical for promoting the overgrowth of tumorous discs, we confirmed that *Ilp8* was indeed expressed only in a subset of cells within *scrib* tumors (Figure 7G) and that removing *Ets21C* dramatically reduced the growth of *scrib* tumors (Figure 7H). Thus, while the function of Ets21C seems most essential for regeneration, where it controls the maintenance of a number of pro-regenerative genes, this same GRN is co-opted to support the growth of tumorous imaginal discs (Figure 7I).

Discussion

Imaginal disc regeneration has been previously shown to be driven by increased proliferation and enhanced plasticity in cells that are close to the damaged tissue. Since these blastema cells represent a small subset of cells in the disc, it has been challenging to identify the GRNs that function specifically during regeneration. Using single-cell transcriptomics, we have identified and characterized cellular states that are unique to regenerating tissues as compared to normal development. We have found that the blastema of regenerating discs is composed of at least two distinct cellular states, Blastema1 and Blastema2, with Blastema1 cells being surrounded by Blastema2. We have shown that these cell states are not immutable properties of cells; rather, cells can transition between these states during the course of regeneration. Moreover, proximal cells can be recruited into a blastema state, and as regeneration progresses, both Blastema1 and Blastema2 cells can adopt non-blastema states in order to contribute to the regenerated tissue. Thus, these blastema cells represent

transitional states that promote regenerative growth and ultimately undergo regenerative repatterning.

The blastema cells express several genes that encode secreted proteins such as Upd3, Mmp1, Ilp8, and Aspr, and seem to function in ways that are similar to regeneration-organizing cells that have been described recently in vertebrates [13]. Importantly, we have shown that the transcription factor Ets21C plays a crucial role in maintaining expression of many of these genes for enough time to allow regeneration to proceed to completion. The JNK/AP-1 pathway has been shown to be a key activator of regenerative growth but its activity declines prior to the completion of regeneration. By forming a type 1 coherent feed-forward loop with Ets21C, the JNK/AP-1 pathway can sustain expression of pro-regenerative genes after AP-1 activity has decreased. Ets21C function is also necessary for slowing down development both locally in the disc as well as systemically. In its absence, regeneration concludes prematurely and early differentiation occurs. The roles of mammalian orthologs of *Ets21C*, *ERG* and *FLI1*, in regeneration clearly deserve further study. Regeneration-specific GRNs may also exist in vertebrates and their reactivation and maintenance could be valuable for regenerative medicine.

Finally, we have also observed similarities between the regeneration blastema and subsets of cells in tumorous imaginal discs. In support of this, we find that *Ets21C* is required for both regenerative growth and the overgrowth of *scrib* mutant discs. Thus, as during regeneration, *Ets21C* and its mammalian orthologs may function in subsets of tumor cells to sustain tumorigenic growth. This would provide additional support for the hypothesis that cancers are akin to wounds that do not heal [59], suggesting that the investigation of pro-regenerative GRNs in oncogenesis merits further exploration.

STAR Methods

Resource Availability

Lead contact—Further information and requests for resources and reagents should be directed to and will be fulfilled by the lead contact, Iswar K. Hariharan (ikh@berkeley.edu).

Materials availability—This study did not generate new unique reagents.

Data and code availability

- Single-cell RNA-seq data have been deposited at GEO and are publicly available as of the date of publication. Accession numbers are listed in the key resources table.
- All original code has been deposited at GitHub and is publicly available as of the date of publication. DOIs are listed in the key resources table.
- Any additional information required to reanalyze the data reported in this paper is available from the lead contact upon request.

Experimental Model and Subject Detail

Drosophila strains—*Drosophila* stocks and crosses were maintained in standard conditions on Bloomington food. Stocks were maintained at room temperature. For regeneration experiments including pupariation timings, eggs were collected on grape plates for 6–8 hours and 55 L1 larvae were transferred into Bloomington food vials supplemented with yeast paste. See additional notes about experimental conditions under ***Regeneration experiments***. The stocks that were used in this study include: *Ets21C*$^{\Delta 10}$ [39]; *UAS-Ets21C (UAS-Ets21C-long)* [39]; *UAS-Ets21C-RNAi* [39]; *eyFLP; arm-lacZ FRT40A; hsFLP; FRT40A ; hsFLP; FRT40A ubi-RFP; rn-GAL4, tub-GAL80*^{ts}, *UAS-egr* (Bl51280) [7]; *rn-GAL4, tub-GAL80*^{ts}, *UAS-rpr* [7]; *UAS-his::RFP* [60] ; *scrib*^{1} [61]; *scrib*^{2} [57]; and *Him-GFP* [62]. Stocks obtained from the Bloomington Stock Center include: *Ilp8-GFP (Ilp8*^{MI00727}, Bl33079); *Ets21C-GFP* (*Pbac-Ets21C-GFP.FLAG*^{VK00033}, Bl38639); *hh-Gal4; hh-Gal4, UAS-GFP*^{nls}; *rn-Gal4* (Bl7405); *Df(2L)BSC107 (Bl8673); Df(2L)BSC456* (Bl24960); *UAS-hep*^{wt} (Bl9308); *UAS-kay-RNAi (*Bl33379); *UAS-JNK*^{DN} (Bl9311); *Ubi-FRT-stop-FRT-GFP*^{nls} (BL32251)[63]; *lexAOp-FLP* (Bl55819); *lexAOp-RFP-membrane; GMR26E03-lexA* (Bl54354)[64]; *3XUAS-FLP.G5.PEST* (Bl55809); *AP-1-GFP* reporter (Bl59010)[65].

Methods Details

Genotypes—The two genetic ablation systems used in the paper (1) *rn-GAL4, tub-GAL80*^{ts}, *UAS-egr* and (2) *rn-GAL4, tub-GAL80*^{ts}, *UAS-rpr* will be abbreviated (1) *rn*^{TS}*>egr* and (2) *rn*^{TS}*>rpr.* The genotype of the wing discs from the following: Figures 1H, 1J, 2E–G: *rn*^{TS}*>egr / Ilp8-GFP.* Figure 2A–C**:** *Ubi-FRT-stop-FRT-GFP*^{nls}; *rn*^{TS}*>egr / 3XUAS-FLP.G5.PEST*. Figure 2J–K *rn*^{TS}*>egr/ +*. Figure 2L: *GMR26E03-lexA / lexAOp-RFP-membrane; Ilp8-GFP / +*. Figure 1M**:** *GMR26E03-lexA, lexAOp-FLP, Ubi-FRT-stop-FRT-GFP*^{nls}. Figure 2N: *GMR26E03-lexA / lexAOp-RFP-membrane; Ilp8-GFP/ rn*^{TS}*>egr*. Figure 2O**:** *GMR26E03-lexA, lexAOp-FLP, Ubi-FRT-stop-FRT-GFP*^{nls}*/ rn*^{TS}*>egr.* Figure 3B**:** *Ets21C-GFP*. Figures 3C, 6F–J**:** *Ets21C-GFP/ rn*^{TS}*>egr*. Figure 3D**:** *rn-GAL4 / Ets21C-GFP, UAS-his::RFP.* Figures 4E–I, 5A–E, 5I–J, S4A–B**:** Wild type = +/+; *rn*^{TS}*>egr/ +, Ets21C*$^{-/-}$ *= Ets21C*$^{\Delta 10/\Delta 10}$; *rn*^{TS}*>egr/ +*. Figure 6A–E**:** *AP-1 activity reporter-GFP/ rn*^{TS}*>egr.* Figure 7G**:** *+/+; scrib*^{1} *Ilp8-GFP / scrib*^{2}. Figure 7H**:** *Ets21C*$^{\Delta 10/\Delta 10}$; *scrib*^{1} *Ilp8-GFP / scrib*^{2}. Figure S3C**:** *UAS-hep*^{wt}; *rn-GAL4/ Ets21C-GFP.* Figure S3D**:** *rn*^{TS}*>rpr /UAS-GFP*^{nls}. Figure S3E**:** *rn*^{TS}*>rpr /UAS-JNK*^{DN}. Figure S4D**:** *hsFLP; Ets21C*$^{\Delta 10}$ *FRT40A / ubi-RFP FRT40A; rn*^{TS}*>egr / Ilp8-GFP.*

Regeneration experiments—Unless otherwise noted, the genetic ablation system used to study regeneration was *rn-GAL4, tub-GAL80*^{ts}, *UAS-eiger* [7]. Genetic ablation experiments were conducted by synchronizing development by collecting eggs on grape plates and picking 55 L1 larvae into vials with yeast paste. Temperature shifts to induce ablation (from 18 °C to 30 °C) were conducted on day 7 after egg lay (AEL) for 40 hours. Wing discs were dissected at several time points during regeneration, starting at halfway through the ablation period (A½), during the start of the regeneration phase (R0), and after 24, 48 or 72 h of regeneration (R24, R48, R72) (Figure S1A). The extent of adult wing regeneration was scored by binning the resulting wings into 5 categories (0%, 25%, 50%, 75%, and 100%)[7]. The resulting regeneration scores were calculated per population.

Experimental replicates were done on separate days with a minimum of 2 vials per genotype and three replicates per genotype.

Immunohistochemistry and imaging—The following antibodies were from the Developmental Studies Hybridoma Bank (DSHB): mouse anti-Wg (1:100, 4D4), mouse anti-Mmp1 (1:100, a combination of 14A3D2, 3A6B4 and 5H7B11), mouse anti-Nubbin (Nub 2A) (1:10), and rat anti-Elav (1:50, Elav-7E8A10). The following antibodies were gifts: rat anti-Zfh2[66] (1:100, Chris Doe), rat anti-Twist (1:1000, Eric Wieschaus), and rat anti-Pvf1[67] (1:500, Ben-Zion Shilo). The following antibodies are from commercial sources: rabbit anti-cleaved Death caspase-1 (Dcp-1) (1:250, Cell Signaling); chicken anti-GFP (1:500, ab13970 Abcam, Cambridge, UK); rabbit anti-PHH3 (1:500, Millipore-Sigma). Secondary antibodies were from Cell Signaling. Nuclear staining with DAPI (1:1000). Tissues were imaged on a Zeiss Axioplan microscope with Apotome attachment, using 10x and 20x objectives. Image files were processed with ImageJ software [68].

In Situ Hybridization Chain Reaction—*In situ* hybridization chain reaction (HCR) was performed on wing discs based on HCR v3.0 protocol [36,69], excluding methanol dehydration. Briefly, regenerating and non-regenerating larvae were dissected, fixed in 4% paraformaldehyde and washed with 1x PBS. Discs were then permeabilized and incubated overnight with the RNA probes at 37 °C. Subsequently, the samples were washed and incubated overnight with fluorescently-tagged RNA hairpins and DAPI at room temperature. HCR probes, hairpins, and buffers were ordered from Molecular Instruments.

EdU assay—For EdU staining, live discs were incubated in Schneider's medium (ThermoFisher 21720024) with EdU for 30 minutes, following the protocol for the Click-iT EdU Cell Proliferation Kit, Alexa Fluor 555 (ThermoFisher C10338) and Alexa Fluor 647 (ThermoFisher C10340). After the incubation, discs were fixed in 4% paraformaldehyde for 15 min, before proceeding with standard antibody staining, as detailed above.

Mitotic clones during regeneration—Mosaic tissues were generated by recombinase-driven (FLP/FRT) mitotic recombination within the genetic background of the ablation system. The expression of *hsFLP* was induced by an 1h heat-shock at 37 °C on day 3 AEL, which generated clones throughout the imaginal discs prior to genetic ablation and regeneration. Mutant cells were labeled by the absence of RFP and wild-type cells were marked by 2X RFP. The genotype of the experimental larvae used to generate *Ets21C* mutant clones during regeneration: *hsFLP; Ets21C$^{\Delta 10}$, FRT40A / ubi-RFPnls, FRT40A; rn-GAL4, tub-GAL80^{ts}, UAS-eiger / Ilp8-GFP* (Figure S4D).

Lineage-tracing experiments—We identify an enhancer for the gene *grain (grn)* that was primarily expressed in the inner-hinge, G*MR26E03-lexA* [64] during normal development (Figure 2L, M). Lineage-tracing was performed by permanently labeling the cells that expressed *GMR26E03-lexA* by driving the expression of the recombinase FLP (*lexAop-FLP*) to induce the removal of a stop-cassette (*Ubi-FRT-stop-FRT-GFP^{nls})* (Figure 2M, O).

Pupariation timing experiments—Images were taken every 20 minutes of vials that contained animals as they transitioned between larva to pupa. This was performed at 18

°C with a wide-angle camera (Arducam). Pupariation was scored by observing when the animals stopped moving and darken in color.

Physical wounding assay—Wing discs were physically wounded *in situ* as described in [70]. Briefly, L3 larvae with the wing pouch fluorescently labeled (*rn-GAL4, UAS-his::RFP)* were visualized using a fluorescence microscope. The right wing pouch was wounded by carefully applying pressure on the larval cuticle using a thin gauge insulin needle without penetrating the larval cuticle. Larvae were then returned to vials containing Bloomington food and dissected 6 hours or 24 hours later.

Single-cell data collection—A total of 4 single-cell RNA sequencing datasets were produced within this study: two replicates for wild-type regeneration and two replicates for *Ets21C*$^{-/-}$ regeneration. For each sample, approximately 300 regenerating wing-imaginal discs were collected after 24 hours of regeneration (R24). Discs were dissected within 1 hour in Supplemented Schneider's Medium. Both wild-type regeneration samples and one *Ets21C*$^{-/-}$ sample were processed according to the protocol outlined in [19], using a mixture of trypsin and collagenase to enzymatically dissociate the tissues at room temperature. The second *Ets21C*$^{-/-}$ regeneration sample was dissociated with 0.25% Trypsin-EDTA solution at 37 °C, similar to the protocol described in [22] but using Rinaldini solution for washes. After dissociation, we used FACS to eliminate both apoptotic cells, cellular debris, and cell aggregations for all samples. Because we often observed an enrichment of myoblasts after dissociation, we sorted out myoblasts during the collection of our second wild-type regeneration sample and both *Ets21C*$^{-/-}$ samples. This was done with a *Holes in muscle (Him)-GFP* construct that specifically labeled the myoblasts [62]. Single-cell suspensions were barcoded for single-cell RNA sequencing with the 10X Chromium Single Cell platform (v2 chemistry for wild-type regeneration samples, v3.1 chemistry for *Ets21C*$^{-/-}$ regeneration samples. All barcoded libraries were sequenced on an Illumina NovaSeq to over 60% saturation.

Quantification and Statistical Analysis

Fluorescence intensity quantification—We used the ImageJ/FIJI [68] software to quantify immunohistochemistry and HCR fluorescence intensity within microscopy images. Fluorescence intensity was manually thresholded into binary values, and the fluorescence area of representative disc proper slices was calculated. For comparing changes in fluorescence area between conditions, statistical significance was determined either via t-test or Wilcoxon test as noted in Figure Legends.

EdU assay quantification—EdU intensity was quantified using the ImageJ software [68]. For each regenerating disc, a square box was drawn, centered around the blastema. The length of the box was 140 microns for the R0 discs and 160 microns for the R24 discs. The EdU intensity was measured at every pixel along the two diagonals of each box using ImageJ's "Plot Profile" function. Subsequent analysis was done using R software. The measured EdU intensities were first z-normalized (i.e., for all values in a measured profile, subtract the mean and divide by the standard deviation) and then averaged across all diagonals from all processed discs at each regenerating time point. The average normalized

(scaled) EdU intensity was plotted with the package ggplot2, and smoothed curves were added using the stat_smooth function with method = "gam".

Single-cell data analysis of wild-type regeneration—Single-cell sequencing reads for wild-type regeneration samples were aligned with the 10x Genomics CellRanger [71] pipeline (v.2.2.0) to the *Drosophila melanogaster* transcriptome (version 6.24, FlyBase [72]). Analysis of the single-cell data (filtered matrices produced by CellRanger [71]) was conducted in the R and Python [73] programming languages, primarily using the packages scvi-tools v0.9.1 [20,21,74], Seurat v3 [75], and Scanpy [76].

We used scvi-tools[21] to harmonize our single-cell data from regenerating wing discs with the single-cell data from developing wild-type wing discs presented in our previous study (accession number GSE155543)[19]. We used Seurat's variance-stabilizing transformation method to select 1000 variable genes for each batch, and the scVI VAE model (from scvi-tools [21]) was trained on the union of these genes (see GitHub code for details). The scVI latent space was used as the input for Seurat's Louvain clustering algorithm, and known transcriptional markers were used to classify cell clusters: *SPARC* and *twist* for myoblasts, *Fasciclin 3 (Fas3)* and *narrow* for the disc epithelium, and *regucalcin* and *Hemese (He)* for hemocytes (Figure S1). We removed an AMP-epithelium doublet cluster that expressed both AMP and epithelium markers, possessed elevated average nGene and nUMI counts, and contained a large number of potential doublets as classified by the tool DoubletFinder[77]. We then isolated the disc epithelial cells for subsequent analysis.

We applied quality control filtering to the disc epithelium cells. First, we processed each batch using the Seurat pipeline [75] and removed low-quality clusters. We classified low-quality clusters as having: 1) an average nGene less than 1 standard deviation below the average nGene of all cells, 2) an average percent.mito greater than 1 standard deviation above the average percent.mito of all cells, and 3) an abundance of negative marker genes compared to positive markers genes (as calculated by a Wilcoxon test). After removing low-quality clusters, batches were harmonized with scVI, trained on the union of the top 1000 variable genes (via Seurat[75]) within the epithelium cells for each batch. The scVI latent space was used as a basis for Seurat's Louvain clustering. We removed a cluster that we determined to be epithelium-epithelium doublets, based on the following characteristics: (1) higher average nGene compared to all other clusters, (2) an abundance of potential doublets as classified by DoubletFinder[77] from each batch (~70% of all potential doublets classified were contained within this cluster), and (3) a lack of marker genes (both positive and negative) when compared to other clusters. We also removed a small number of trachea cells based on the expression of marker genes *tracheal-prostasin* and *waterproof*. We re-ran our variable gene selection, scVI harmonization, and Seurat clustering. Data was visualized in 2 dimensions with UMAP [78].

Single-cell comparison of wild-type and Ets21C$^{-/-}$ regeneration samples—Single-cell sequencing reads for *Ets21C*$^{-/-}$ regeneration samples were aligned with the 10x Genomics CellRanger pipeline (v.6.1.0) [71] to the *Drosophila melanogaster* transcriptome (version 6.24, FlyBase [72]). Cells from the filtered barcode matrices produced by CellRanger were subject to additional filtering. First, we processed each *Ets21C*$^{-/-}$ regeneration batch

using the Seurat pipeline and removed low-quality clusters (see classification of low-quality clusters above). Cells were annotated as being derived from the disc epithelium, myoblasts, and hemocytes. DoubletFinder[77] was applied to each batch to identify clusters with a high percentage of predicted doublets, and these clusters were removed. The disc epithelium clusters were isolated from each batch for subsequent analysis.

The epithelium data from wild-type regeneration, wild-type development, and *Ets21C*$^{-/-}$ regeneration samples was initially harmonized with scVI [21], trained on the union of the top 1000 variable genes for each batch as determined by Seurat [75]. The weights from this scVI model were used to initialize a scANVI model for semi-supervised training and label transfer [74] (see GitHub code for details). The cluster identities from our regeneration analysis (Figure 1B) were supplied as input labels to scANVI, with all *Ets21C*$^{-/-}$ regeneration cells marked as "Unknown". After training, the scANVI latent space was used as a basis for UMAP, and the transferred labels corresponded to the highest predicted identity for each *Ets21C*$^{-/-}$ cell by scANVI (Figure 4A).

Single-cell comparison of regenerating and scrib tissues—The expression matrices for the *scrib* single-cell data were downloaded from GEO, accession number GSE130566 [22]. Gene names were updated to match those within our wild-type regeneration and development datasets. All *scrib* datasets (4d, 5d, 8d, and 14d) were harmonized with scVI, trained on the union of the top 1000 variable genes for each batch as determined by Seurat [75]. Louvain clustering was performed using Seurat [75], and we isolated the *scrib* epithelium clusters (identifiable by high expression of *Fasciclin 3* and *narrow*) for subsequent comparison with the regeneration and wild-type epithelium data. No *scrib* epithelium cells were filtered during this comparative analysis.

The epithelium data from wild-type regeneration, wild-type development, and *scrib* samples was harmonized using both scVI (for initial unsupervised training) and scANVI (for subsequent semi-supervised training and label transfer) [21,74] (see application to *Ets21C*$^{-/-}$ data and GitHub code for further details). The cluster identities from our regeneration analysis (Figure 1B) were supplied as input labels to scANVI, with all *scrib* cells marked as "Unknown". After training, the scANVI latent space was used as a basis for UMAP (Figure 7B), and the transferred labels corresponded to the highest predicted identity for each *scrib* cell by scANVI (Figure 7C–F).

Pseudotime analysis of regeneration data—Because we were interested in uncovering transcriptional transitions from the blastema to either hinge or pouch cell fates, we first subset the integrated wild-type regeneration and development datasets to only include cells from these populations (i.e., we removed cells annotated as notum and PE). We identified potential trajectories through these cells with Slingshot [79], using the scVI-generated latent space as the input to the algorithm and indicating Blastema1 as the starting cluster. The algorithm identified 5 potential trajectories, which we grouped into two categories: two trajectories that generally traversed from Blastema1 to Blastema2 to pouch cells, and three trajectories that generally traversed from Blastema1 to Blastema2 to hinge cells. Similar trends were observed among pouch-terminating trajectories and hinge-

terminating trajectories, and we showcase one trajectory from each of these two groups (Figure S2D).

Gene signature analysis of the blastema—For each identity combination (hinge-pouch, pouch-notum, and notum-hinge), gene signatures were constructed as follows: First, differential expression was performed between wild-type (non-regenerating) cells of each identity pair (e.g., for the hinge-pouch signature, differential expression was performed between cells from [19] classified as hinge vs. cells classified as pouch). This was conducted using a Wilcoxon test via Seurat's FindMarkers function[75], selecting genes with a natural-log fold-change of greater than 0.25 and a Bonferroni-corrected p-value of < 0.05. This provided three gene sets that differentiated hinge-pouch, pouch-notum, and notum-hinge identities. Second, principal component analysis was performed on all cells using each gene set. The first principal components from each analysis were defined as the gene signatures, as they best separated cells of the different identities.

Gene signature of cellular maturity—To determine the relative cellular maturity (or developmental progression) of individual cells within the regenerating tissue, we first selected genes with differential expression between all epithelial cells from the mid (96h) and late (120h) 3rd instar development scRNAseq datasets[19] (above natural log fold-change > 0.15 and a Bonferroni-corrected p-value < 0.05 calculated via Wilcoxon test). These gene sets were used to perform principal component analysis on the wild-type development scRNAseq data. We extracted the first principal component, as it best separated cells from the mid and late developmental time points. The genes and their corresponding weights that comprised this first principal component were used as the basis for our maturity signature. We applied this signature as a linear combination to cells from the wild-type and *Ets21C*$^{-/-}$ datasets to determine their maturity scores, which were visualized on a violin plot (Figure 5G).

Supplementary Material

Refer to Web version on PubMed Central for supplementary material.

Acknowledgments:

The authors would like to thank Mirka Uhlirova, Ben-Zion Shilo, David Bilder, Chris Doe, and Eric Wieschaus for stocks and reagents, current and former members of the Hariharan and Yosef labs for feedback, David Bilder and Craig Miller for helpful feedback on the manuscript, Joel Sadler for computational assistance, and the Bloomington Stock Center, DRSC/TRiP Functional Genomics Resources, and Developmental Studies Hybridoma Bank for stocks and reagents. Funding was from NIH R35 GM122490 (IKH). NY was a Chan Zuckerberg Biohub investigator.

References:

1. Vogg MC, Buzgariu W, Suknovic NS, and Galliot B (2021). Cellular, Metabolic, and Developmental Dimensions of Whole-Body Regeneration in Hydra. Cold Spring Harb Perspect Biol 13. 10.1101/cshperspect.a040725.
2. Reddien PW (2022). Positional Information and Stem Cells Combine to Result in Planarian Regeneration. Cold Spring Harb Perspect Biol 14. 10.1101/cshperspect.a040717.

3. Aztekin C, and Storer MA (2022). To regenerate or not to regenerate: Vertebrate model organisms of regeneration-competency and -incompetency. Wound Repair Regen. 10.1111/wrr.13000.
4. Otsuki L, and Tanaka EM (2021). Positional Memory in Vertebrate Regeneration: A Century's Insights from the Salamander Limb. Cold Spring Harb Perspect Biol. 10.1101/cshperspect.a040899.
5. Muneoka K, Fox WF, and Bryant SV (1986). Cellular contribution from dermis and cartilage to the regenerating limb blastema in axolotls. Dev Biol 116, 256–260. 10.1016/0012-1606(86)90062-x. [PubMed: 3732605]
6. Hadorn E, Bertani G, and Gallera J (1949). Regulative capacity and field organization of male genital discs in *Drosophila melanogaster*. Roux's Arch Dev Biol 144, 31–70. 10.1007/BF00575293.
7. Smith-Bolton RK, Worley MI, Kanda H, and Hariharan IK (2009). Regenerative growth in *Drosophila* imaginal discs is regulated by Wingless and Myc. Dev Cell 16, 797–809. 10.1016/j.devcel.2009.04.015. [PubMed: 19531351]
8. Bergantiños C, Corominas M, and Serras F (2010). Cell death-induced regeneration in wing imaginal discs requires JNK signalling. Development 137, 1169–1179. 10.1242/dev.045559. [PubMed: 20215351]
9. Abbott LC, Karpen GH, and Schubiger G (1981). Compartmental restrictions and blastema formation during pattern regulation in *Drosophila* imaginal leg discs. Dev Biol 87, 64–75. 10.1016/0012-1606(81)90061-0. [PubMed: 7286422]
10. Klebes A, Sustar A, Kechris K, Li H, Schubiger G, and Kornberg TB (2005). Regulation of cellular plasticity in *Drosophila* imaginal disc cells by the Polycomb group, trithorax group and lama genes. Development 132, 3753–3765. 10.1242/dev.01927. [PubMed: 16077094]
11. Khan SJ, Abidi SNF, Skinner A, Tian Y, and Smith-Bolton RK (2017). The *Drosophila* Duox maturation factor is a key component of a positive feedback loop that sustains regeneration signaling. PLoS Genet 13, e1006937. 10.1371/journal.pgen.1006937. [PubMed: 28753614]
12. Gerber T, Murawala P, Knapp D, Masselink W, Schuez M, Hermann S, Gac-Santel M, Nowoshilow S, Kageyama J, Khattak S, et al. (2018). Single-cell analysis uncovers convergence of cell identities during axolotl limb regeneration. Science 362. 10.1126/science.aaq0681.
13. Aztekin C, Hiscock TW, Marioni JC, Gurdon JB, Simons BD, and Jullien J (2019). Identification of a regeneration-organizing cell in the Xenopus tail. Science 364, 653–658. 10.1126/science.aav9996. [PubMed: 31097661]
14. Goldman JA, and Poss KD (2020). Gene regulatory programmes of tissue regeneration. Nat Rev Genet 21, 511–525. 10.1038/s41576-020-0239-7. [PubMed: 32504079]
15. Worley MI, and Hariharan IK (2021). Imaginal Disc Regeneration: Something Old, Something New. Cold Spring Harb Perspect Biol. 10.1101/cshperspect.a040733.
16. Fox DT, Cohen E, and Smith-Bolton R (2020). Model systems for regeneration: Drosophila. Development 147, dev173781. 10.1242/dev.173781. [PubMed: 32253254]
17. Herrera SC, Martín R, and Morata G (2013). Tissue homeostasis in the wing disc of *Drosophila melanogaster*: immediate response to massive damage during development. PLoS Genet 9, e1003446. 10.1371/journal.pgen.1003446. [PubMed: 23633961]
18. Karpen GH, and Schubiger G (1981). Extensive regulatory capabilities of a *Drosophila* imaginal disk blastema. Nature 294, 744–747. 10.1038/294744a0. [PubMed: 6798471]
19. Everetts NJ, Worley MI, Yasutomi R, Yosef N, and Hariharan IK (2021). Single-cell transcriptomics of the *Drosophila* wing disc reveals instructive epithelium-to-myoblast interactions. Elife 10, e61276. 10.7554/eLife.61276. [PubMed: 33749594]
20. Lopez R, Regier J, Cole MB, Jordan MI, and Yosef N (2018). Deep generative modeling for single-cell transcriptomics. Nat Methods 15, 1053–1058. 10.1038/s41592-018-0229-2. [PubMed: 30504886]
21. Gayoso A, Steier Z, Lopez R, Regier J, Nazor KL, Streets A, and Yosef N (2021). Joint probabilistic modeling of single-cell multi-omic data with totalVI. Nat Methods 18, 272–282. 10.1038/s41592-020-01050-x. [PubMed: 33589839]
22. Deng M, Wang Y, Zhang L, Yang Y, Huang S, Wang J, Ge H, Ishibashi T, and Yan Y (2019). Single cell transcriptomic landscapes of pattern formation, proliferation and growth in *Drosophila* wing imaginal discs. Development 146, dev179754. 10.1242/dev.179754. [PubMed: 31455604]

23. Bageritz J, Willnow P, Valentini E, Leible S, Boutros M, and Teleman AA (2019). Gene expression atlas of a developing tissue by single cell expression correlation analysis. Nat Methods 16, 750–756. 10.1038/s41592-019-0492-x. [PubMed: 31363221]
24. Zappia MP, de Castro L, Ariss MM, Jefferson H, Islam AB, and Frolov MV (2020). A cell atlas of adult muscle precursors uncovers early events in fibre-type divergence in *Drosophila*. EMBO Rep 21, e49555. 10.15252/embr.201949555. [PubMed: 32815271]
25. Schubiger M, Sustar A, and Schubiger G (2010). Regeneration and transdetermination: the role of wingless and its regulation. Dev Biol 347, 315–324. 10.1016/j.ydbio.2010.08.034. [PubMed: 20816798]
26. Harris RE, Setiawan L, Saul J, and Hariharan IK (2016). Localized epigenetic silencing of a damage-activated WNT enhancer limits regeneration in mature *Drosophila* imaginal discs. Elife 5, e11588. 10.7554/eLife.11588. [PubMed: 26840050]
27. McClure KD, Sustar A, and Schubiger G (2008). Three genes control the timing, the site and the size of blastema formation in *Drosophila*. Dev Biol 319, 68–77. 10.1016/j.ydbio.2008.04.004. [PubMed: 18485344]
28. Katsuyama T, Comoglio F, Seimiya M, Cabuy E, and Paro R (2015). During *Drosophila* disc regeneration, JAK/STAT coordinates cell proliferation with Dilp8-mediated developmental delay. Proc Natl Acad Sci U S A 112, E2327–2336. 10.1073/pnas.1423074112. [PubMed: 25902518]
29. Harris RE, Stinchfield MJ, Nystrom SL, McKay DJ, and Hariharan IK (2020). Damage-responsive, maturity-silenced enhancers regulate multiple genes that direct regeneration in *Drosophila*. Elife 9, e58305. 10.7554/eLife.58305. [PubMed: 32490812]
30. La Fortezza M, Schenk M, Cosolo A, Kolybaba A, Grass I, and Classen AK (2016). JAK/STAT signalling mediates cell survival in response to tissue stress. Development 143, 2907–2919. 10.1242/dev.132340. [PubMed: 27385008]
31. Santabarbara-Ruiz P, Lopez-Santillan M, Martinez-Rodriguez I, Binagui-Casas A, Perez L, Milan M, Corominas M, and Serras F (2015). ROS-Induced JNK and p38 Signaling Is Required for Unpaired Cytokine Activation during *Drosophila* Regeneration. PLoS Genet 11, e1005595. 10.1371/journal.pgen.1005595. [PubMed: 26496642]
32. Worley MI, Alexander LA, and Hariharan IK (2018). CtBP impedes JNK- and Upd/STAT-driven cell fate misspecifications in regenerating *Drosophila* imaginal discs. Elife 7, e30391. 10.7554/eLife.30391. [PubMed: 29372681]
33. Wu Y, Brock AR, Wang Y, Fujitani K, Ueda R, and Galko MJ (2009). A blood-borne PDGF/VEGF-like ligand initiates wound-induced epidermal cell migration in Drosophila larvae. Curr Biol 19, 1473–1477. 10.1016/j.cub.2009.07.019. [PubMed: 19646875]
34. Currie JD, Kawaguchi A, Traspas RM, Schuez M, Chara O, and Tanaka EM (2016). Live Imaging of Axolotl Digit Regeneration Reveals Spatiotemporal Choreography of Diverse Connective Tissue Progenitor Pools. Dev Cell 39, 411–423. 10.1016/j.devcel.2016.10.013. [PubMed: 27840105]
35. Johnson GL, Masias EJ, and Lehoczky JA (2020). Cellular Heterogeneity and Lineage Restriction during Mouse Digit Tip Regeneration at Single-Cell Resolution. Dev Cell 52, 525–540 e525. 10.1016/j.devcel.2020.01.026. [PubMed: 32097654]
36. Choi HMT, Schwarzkopf M, Fornace ME, Acharya A, Artavanis G, Stegmaier J, Cunha A, and Pierce NA (2018). Third-generation in situ hybridization chain reaction: multiplexed, quantitative, sensitive, versatile, robust. Development 145. 10.1242/dev.165753.
37. Cosolo A, Jaiswal J, Csordas G, Grass I, Uhlirova M, and Classen AK (2019). JNK-dependent cell cycle stalling in G2 promotes survival and senescence-like phenotypes in tissue stress. Elife 8, e41036. 10.7554/eLife.41036. [PubMed: 30735120]
38. Verghese S, and Su TT (2016). *Drosophila* Wnt and STAT Define Apoptosis-Resistant Epithelial Cells for Tissue Regeneration after Irradiation. PLoS Biol 14, e1002536. 10.1371/journal.pbio.1002536. [PubMed: 27584613]
39. Mundorf J, Donohoe CD, McClure CD, Southall TD, and Uhlirova M (2019). Ets21c Governs Tissue Renewal, Stress Tolerance, and Aging in the Drosophila Intestine. Cell Rep 27, 3019–3033 e3015. 10.1016/j.celrep.2019.05.025. [PubMed: 31167145]

40. Dobson AJ, Boulton-McDonald R, Houchou L, Svermova T, Ren Z, Subrini J, Vazquez-Prada M, Hoti M, Rodriguez-Lopez M, Ibrahim R, et al. (2019). Longevity is determined by ETS transcription factors in multiple tissues and diverse species. PLoS Genet 15, e1008212. 10.1371/journal.pgen.1008212. [PubMed: 31356597]
41. Kar A, and Gutierrez-Hartmann A (2013). Molecular mechanisms of ETS transcription factor-mediated tumorigenesis. Crit Rev Biochem Mol Biol 48, 522–543. 10.3109/10409238.2013.838202. [PubMed: 24066765]
42. Külshammer E, Mundorf J, Kilinc M, Frommolt P, Wagle P, and Uhlirova M (2015). Interplay among Drosophila transcription factors Ets21c, Fos and Ftz-F1 drives JNK-mediated tumor malignancy. Dis Model Mech 8, 1279–1293. 10.1242/dmm.020719. [PubMed: 26398940]
43. Toggweiler J, Willecke M, and Basler K (2016). The transcription factor Ets21C drives tumor growth by cooperating with AP-1. Sci Rep 6, 34725. 10.1038/srep34725. [PubMed: 27713480]
44. Jin Y, Ha N, Fores M, Xiang J, Glasser C, Maldera J, Jimenez G, and Edgar BA (2015). EGFR/Ras Signaling Controls Drosophila Intestinal Stem Cell Proliferation via Capicua-Regulated Genes. PLoS Genet 11, e1005634. 10.1371/journal.pgen.1005634. [PubMed: 26683696]
45. Bosch M, Serras F, Martin-Blanco E, and Baguna J (2005). JNK signaling pathway required for wound healing in regenerating *Drosophila* wing imaginal discs. Dev Biol 280, 73–86. 10.1016/j.ydbio.2005.01.002. [PubMed: 15766749]
46. Mattila J, Omelyanchuk L, Kyttala S, Turunen H, and Nokkala S (2005). Role of Jun N-terminal Kinase (JNK) signaling in the wound healing and regeneration of a *Drosophila melanogaster* wing imaginal disc. Int J Dev Biol 49, 391–399. 10.1387/ijdb.052006jm. [PubMed: 15968584]
47. Boulan L, Andersen D, Colombani J, Boone E, and Leopold P (2019). Inter-Organ Growth Coordination Is Mediated by the Xrp1-Dilp8 Axis in Drosophila. Dev Cell 49, 811–818 e814. 10.1016/j.devcel.2019.03.016. [PubMed: 31006647]
48. Colombani J, Andersen DS, and Leopold P (2012). Secreted peptide Dilp8 coordinates *Drosophila* tissue growth with developmental timing. Science 336, 582–585. 10.1126/science.1216689. [PubMed: 22556251]
49. Garelli A, Gontijo AM, Miguela V, Caparros E, and Dominguez M (2012). Imaginal discs secrete insulin-like peptide 8 to mediate plasticity of growth and maturation. Science 336, 579–582. 10.1126/science.1216735. [PubMed: 22556250]
50. Romão D, Muzzopappa M, Barrio L, and Milán M (2021). The Upd3 cytokine couples inflammation to maturation defects in *Drosophila*. Curr Biol 31, 1780–1787 e1786. 10.1016/j.cub.2021.01.080. [PubMed: 33609452]
51. Halme A, Cheng M, and Hariharan IK (2010). Retinoids regulate a developmental checkpoint for tissue regeneration in *Drosophila*. Curr Biol 20, 458–463. 10.1016/j.cub.2010.01.038. [PubMed: 20189388]
52. Hackney JF, Zolali-Meybodi O, and Cherbas P (2012). Tissue damage disrupts developmental progression and ecdysteroid biosynthesis in *Drosophila*. PLoS One 7, e49105. 10.1371/journal.pone.0049105. [PubMed: 23166607]
53. Skinner A, Khan SJ, and Smith-Bolton RK (2015). Trithorax regulates systemic signaling during *Drosophila* imaginal disc regeneration. Development 142, 3500–3511. 10.1242/dev.122564. [PubMed: 26487779]
54. Jaszczak JS, and Halme A (2016). Arrested development: coordinating regeneration with development and growth in *Drosophila melanogaster*. Curr Opin Genet Dev 40, 87–94. 10.1016/j.gde.2016.06.008. [PubMed: 27394031]
55. Narbonne-Reveau K, and Maurange C (2019). Developmental regulation of regenerative potential in *Drosophila* by ecdysone through a bistable loop of ZBTB transcription factors. PLoS Biol 17, e3000149. 10.1371/journal.pbio.3000149. [PubMed: 30742616]
56. Alon U (2007). Network motifs: theory and experimental approaches. Nat Rev Genet 8, 450–461. 10.1038/nrg2102. [PubMed: 17510665]
57. Bilder D, Li M, and Perrimon N (2000). Cooperative regulation of cell polarity and growth by Drosophila tumor suppressors. Science 289, 113–116. 10.1126/science.289.5476.113. [PubMed: 10884224]

58. Ji T, Zhang L, Deng M, Huang S, Wang Y, Pham TT, Smith AA, Sridhar V, Cabernard C, Wang J, and Yan Y (2019). Dynamic MAPK signaling activity underlies a transition from growth arrest to proliferation in Drosophila scribble mutant tumors. Dis Model Mech 12. 10.1242/dmm.040147.
59. Dvorak HF (1986). Tumors: wounds that do not heal. Similarities between tumor stroma generation and wound healing. N Engl J Med 315, 1650–1659. 10.1056/NEJM198612253152606. [PubMed: 3537791]
60. Emery G, Hutterer A, Berdnik D, Mayer B, Wirtz-Peitz F, Gaitan MG, and Knoblich JA (2005). Asymmetric Rab 11 endosomes regulate delta recycling and specify cell fate in the Drosophila nervous system. Cell 122, 763–773. 10.1016/j.cell.2005.08.017. [PubMed: 16137758]
61. Bilder D, and Perrimon N (2000). Localization of apical epithelial determinants by the basolateral PDZ protein Scribble. Nature 403, 676–680. 10.1038/35001108. [PubMed: 10688207]
62. Rebeiz M, Reeves NL, and Posakony JW (2002). SCORE: a computational approach to the identification of cis-regulatory modules and target genes in whole-genome sequence data. Site clustering over random expectation. Proc Natl Acad Sci U S A 99, 9888–9893. 10.1073/pnas.152320899. [PubMed: 12107285]
63. Evans CJ, Olson JM, Ngo KT, Kim E, Lee NE, Kuoy E, Patananan AN, Sitz D, Tran P, Do MT, et al. (2009). G-TRACE: rapid Gal4-based cell lineage analysis in Drosophila. Nat Methods 6, 603–605. 10.1038/nmeth.1356. [PubMed: 19633663]
64. Pfeiffer BD, Ngo TT, Hibbard KL, Murphy C, Jenett A, Truman JW, and Rubin GM (2010). Refinement of tools for targeted gene expression in Drosophila. Genetics 186, 735–755. 10.1534/genetics.110.119917. [PubMed: 20697123]
65. Chatterjee N, and Bohmann D (2012). A versatile PhiC31 based reporter system for measuring AP-1 and Nrf2 signaling in Drosophila and in tissue culture. PLoS One 7, e34063. 10.1371/journal.pone.0034063. [PubMed: 22509270]
66. Tran KD, Miller MR, and Doe CQ (2010). Recombineering Hunchback identifies two conserved domains required to maintain neuroblast competence and specify early-born neuronal identity. Development 137, 1421–1430. 10.1242/dev.048678. [PubMed: 20335359]
67. Rosin D, Schejter E, Volk T, and Shilo BZ (2004). Apical accumulation of the Drosophila PDGF/VEGF receptor ligands provides a mechanism for triggering localized actin polymerization. Development 131, 1939–1948. 10.1242/dev.01101. [PubMed: 15056618]
68. Schindelin J, Arganda-Carreras I, Frise E, Kaynig V, Longair M, Pietzsch T, Preibisch S, Rueden C, Saalfeld S, Schmid B, et al. (2012). Fiji: an open-source platform for biological-image analysis. Nature Methods 9, 676–682. 10.1038/nmeth.2019. [PubMed: 22743772]
69. Bruce HS, Jerz G, Kelly SR, McCarthy J, Pomerantz A, Senevirathne G, Sherrard A, Sun DA, Wolff C, and Patel NH (2021). Hybridization Chain Reaction (HCR) In Situ Protocol. . protocols.io. 10.17504/protocols.io.bunznvf6.
70. Yoo SK, Pascoe HG, Pereira T, Kondo S, Jacinto A, Zhang X, and Hariharan IK (2016). Plexins function in epithelial repair in both *Drosophila* and zebrafish. Nat Commun 7, 12282. 10.1038/ncomms12282. [PubMed: 27452696]
71. Zheng GX, Terry JM, Belgrader P, Ryvkin P, Bent ZW, Wilson R, Ziraldo SB, Wheeler TD, McDermott GP, Zhu J, et al. (2017). Massively parallel digital transcriptional profiling of single cells. Nat Commun 8, 14049. 10.1038/ncomms14049. [PubMed: 28091601]
72. Thurmond J, Goodman JL, Strelets VB, Attrill H, Gramates LS, Marygold SJ, Matthews BB, Millburn G, Antonazzo G, Trovisco V, et al. (2019). FlyBase 2.0: the next generation. Nucleic Acids Res 47, D759–D765. 10.1093/nar/gky1003. [PubMed: 30364959]
73. Rossum V (1995). Python reference manual. Department of Computer Science [CS] (R 9525).
74. Xu C, Lopez R, Mehlman E, Regier J, Jordan MI, and Yosef N (2021). Probabilistic harmonization and annotation of single-cell transcriptomics data with deep generative models. Mol Syst Biol 17, e9620. 10.15252/msb.20209620. [PubMed: 33491336]
75. Stuart T, Butler A, Hoffman P, Hafemeister C, Papalexi E, Mauck WM 3rd, Hao Y, Stoeckius M, Smibert P, and Satija R (2019). Comprehensive Integration of Single-Cell Data. Cell 177, 1888–1902 e1821. 10.1016/j.cell.2019.05.031. [PubMed: 31178118]
76. Wolf FA, Angerer P, and Theis FJ (2018). SCANPY: large-scale single-cell gene expression data analysis. Genome Biol 19, 15. 10.1186/s13059-017-1382-0. [PubMed: 29409532]

77. McGinnis CS, Murrow LM, and Gartner ZJ (2019). DoubletFinder: Doublet Detection in Single-Cell RNA Sequencing Data Using Artificial Nearest Neighbors. Cell Syst 8, 329–337 e324. 10.1016/j.cels.2019.03.003. [PubMed: 30954475]

78. McInnes L, Healy J, Saul N, and Großberger L (2018). UMAP: Uniform Manifold Approximation and Projection. Journal of Open Source Software 3, 861. 10.21105/joss.00861.

79. Street K, Risso D, Fletcher RB, Das D, Ngai J, Yosef N, Purdom E, and Dudoit S (2018). Slingshot: cell lineage and pseudotime inference for single-cell transcriptomics. BMC Genomics 19, 477. 10.1186/s12864-018-4772-0. [PubMed: 29914354]

Highlights

- Single-cell analysis identifies regeneration-specific cell states in *Drosophila*
- The transcription factor Ets21C is required for regeneration, not development
- Ets21C sustains a pro-regenerative gene regulatory network in the blastema
- Blastema-like cells are found during tumorous overgrowth

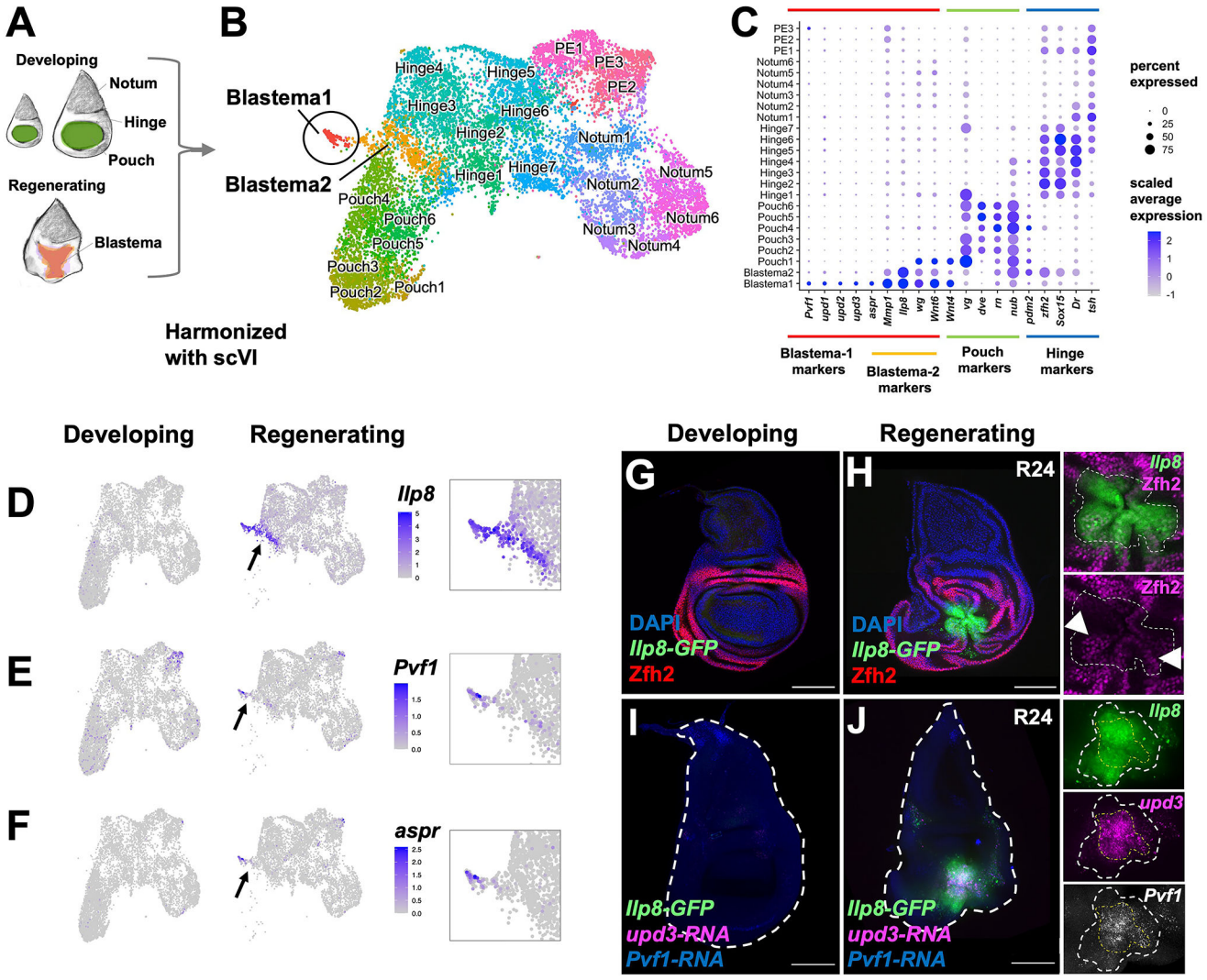

Figure 1. Single-cell analysis reveals two distinct cell states in the regeneration blastema.

(**A**) Diagram of imaginal disc samples compared by scRNAseq. (**B**) UMAP of harmonized regenerating and developing epithelial cells where each point represents an individual cell. See also Figure S1. (**C**) Dot plot summarizing gene expression for cluster marker genes. PE indicates peripodial epithelium. Expression of *Ilp8* (**D**), *Pvf1* (**E**), and *aspr* (**F**) as visualized on UMAP. Arrow points to blastema. (**G-J**) Developing and regenerating wing discs, the latter after 24 h of regeneration (R24) with an *Ilp8-GFP* reporter. (**G, H**) Tissues stained with anti-Zfh2 (hinge marker). Arrowheads point to *Ilp8-GFP*(+) cells that express higher levels of Zfh2. Note that these cells are on the periphery. (**I, J**) Tissues stained with HCR to *Pvf1-RNA* and *upd3-RNA*. In the closeups of the blastema, the area of *Ilp8* and *upd3* are outlined. All microscopy scale bars = 100 μm.

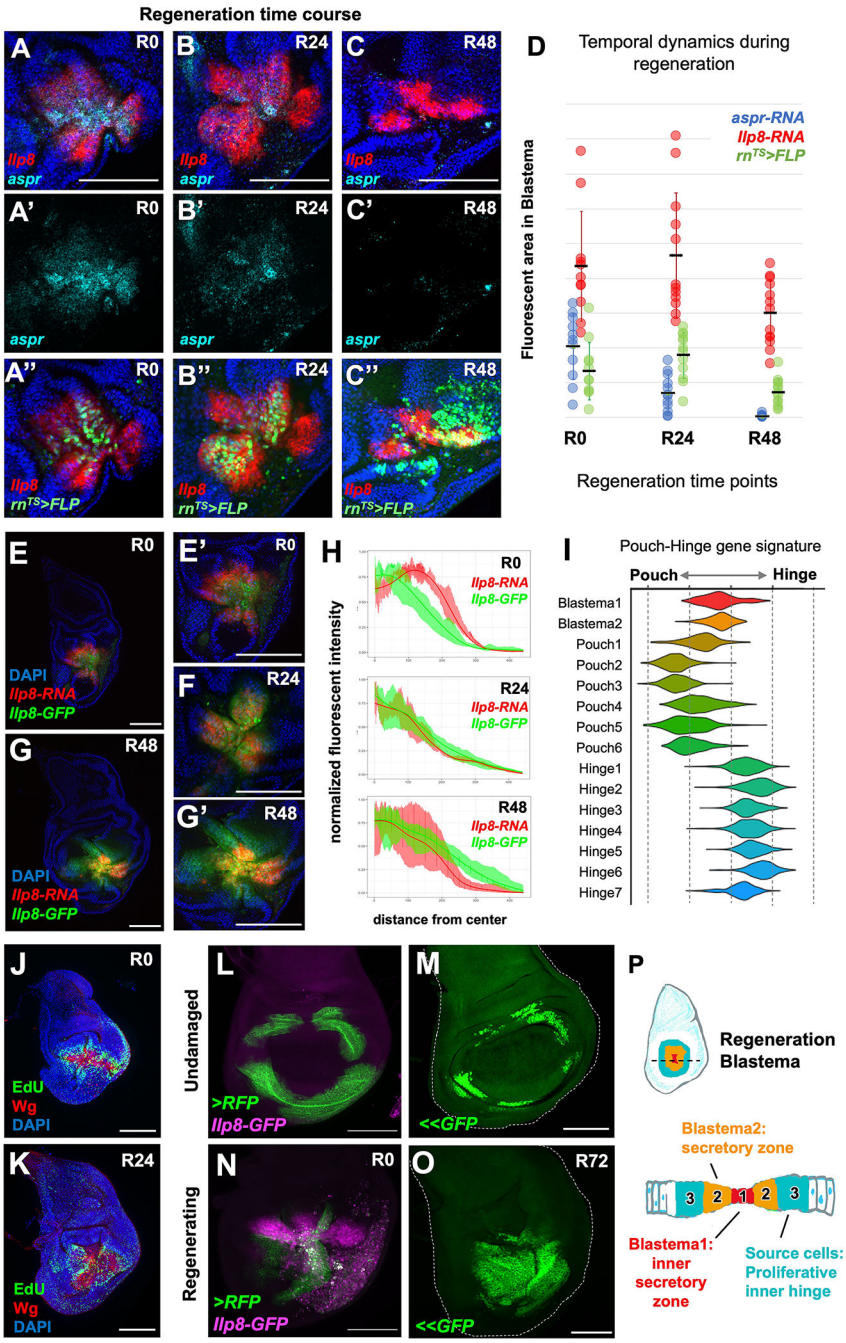

Figure 2. Temporal dynamics of the blastema cellular states during regeneration.

(**A-C**) Time course of regenerating discs with HCR to *aspr-RNA* and *Ilp8-RNA*, with lineage-labeling based on high *rn-GAL4* expression (destabilized *UAS-FLP*). Areas quantified in (**D**). (**E-H**) Regeneration time course of *Ilp8* RNA vs. protein dynamics within the blastema. Note that *Ilp8* expression is expanding at R0 and contracting by R48. Panels (**E**) and (**G**) are shown at higher magnification in panels (**E'**) and (**G'**) respectively. (**I**) Pouch-Hinge gene signature analysis of blastema cell clusters within scRNAseq data. See also Figure S2. (**J, K**) Regenerating wing discs at R0 and R24 with cells in S-phase

visualized by EdU incorporation. (**L-O**) Inner-hinge enhancer during normal development (**L, N**) or during regeneration (**M, O**). Note that (**L, N**) highlights current expression or perdurance of a stable RFP and (**M, O**) shows lineage tracing using a FLP-out GFP (<<GFP). (**P**) Schematic of distinct cell types of the blastema. Microscopy scale bars = 100 μm.

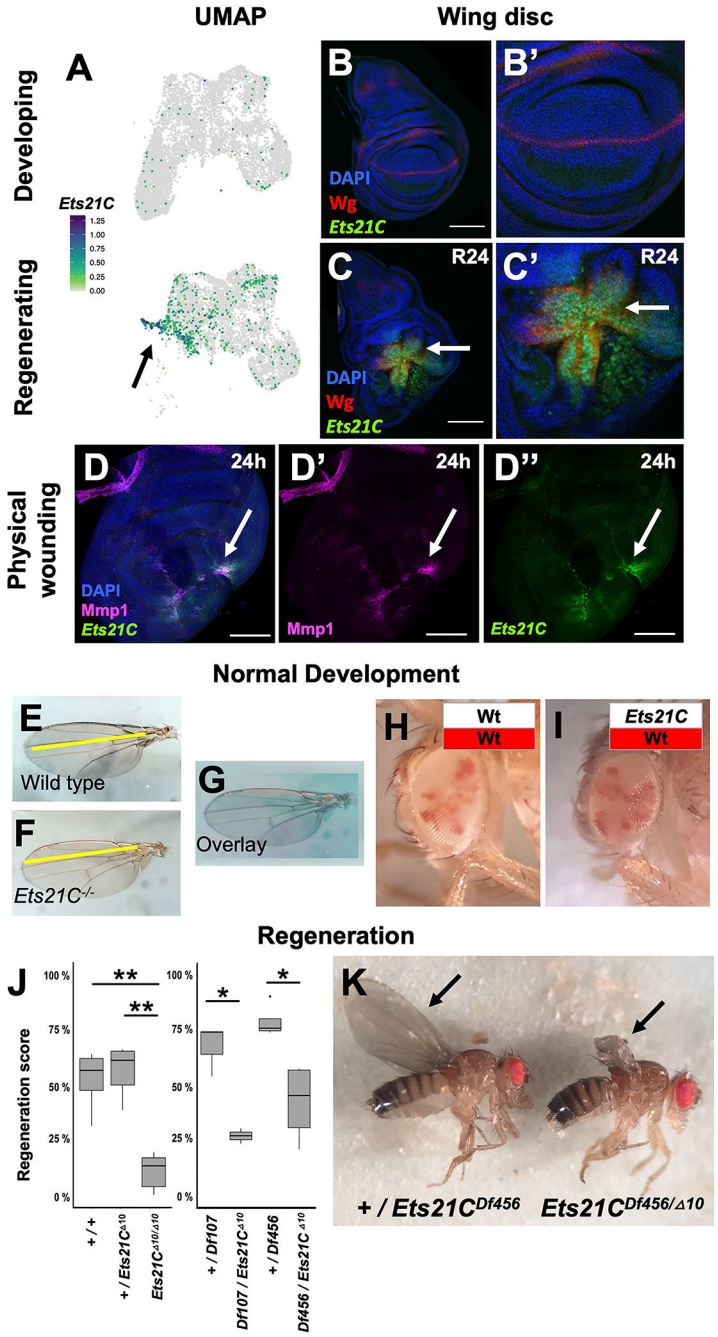

Figure 3. Transcription factor Ets21C is specifically required for regeneration.

(A) *Ets21C* expression in developing and regenerating scRNAseq data. (**B, C**) *Ets21C-GFP* expression in (**B**) developing and (**C**) regenerating wing discs. (**D**) *Ets21C-GFP* expression 24 h after physically wounding disc through larval cuticle. Arrow points to the regions of *Ets21C* expression. (**E-G**) Wing blades from (**E**) wild-type and (**F**) $Ets21C^{-/-}$ mutant animals, raised in standard conditions, and shown overlaid (**G**). (**H, I**) Mosaic adult eyes generated using *eyFLP* with control (**H**) and *Ets21C* (**I**) cells marked by the absence of red pigment. Note that $Ets21C^{-/-}$ mutant cells (**I**) contribute to tissue at a similar proportion as

control cells (**H**). (**J, K**) The extent of regeneration, following genetic ablation as scored by the sizes of the adult wing blades (arrows), p values: * <0.05, ** <0.005 (ANOVA followed by Tukey (left panel), t-test (right panel)). Microscopy scale bars = 100 μm. See also Figure S3.

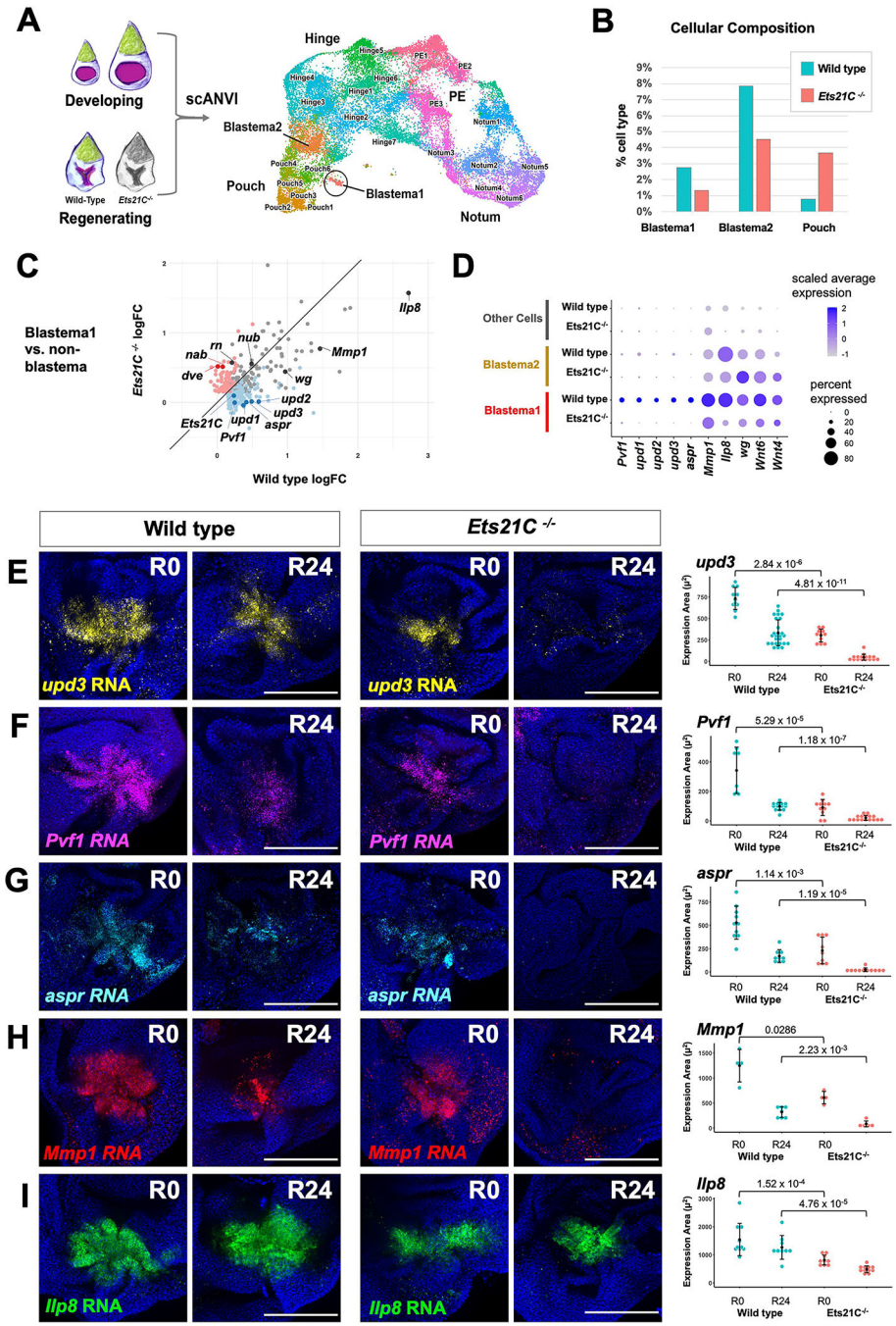

Figure 4. Single-cell analysis reveals genes regulated by *Ets21C* during regeneration.

(**A**) Integration of data from regenerating (R24) *Ets21C*$^{-/-}$ mutant discs with the annotated wild type data shown in Figure 1B. UMAP of harmonized epithelial cells with cell annotations assigned by scANVI. (**B**) Percent cells assigned to Blastema and Pouch clusters. (**C**) Natural-log fold-change (logFC) of differentially expressed genes in Blastema1 cells vs non-Blastema cells for wild type versus *Ets21C*$^{-/-}$ conditions. Blue dots show genes that are significantly (Bonferroni p-value < 0.05) upregulated in Blastema1 cells in wild type but not *Ets21C*$^{-/-}$. Red dots highlight genes that are significantly upregulated in Blastema1

cells in *Ets21C*$^{-/-}$ but not wild type. (**D**) Dot plot summarizing gene expression for blastema cluster marker genes. (**E-I**) Wild type and *Ets21C*$^{-/-}$ mutant discs at early (R0) and mid regeneration (R24) time points with transcripts visualized by HCR as indicated. Area of fluorescence quantified on right with statistical significance between conditions calculated via Wilcoxon test. Microscopy scale bars = 100 μm. See also Figure S4.

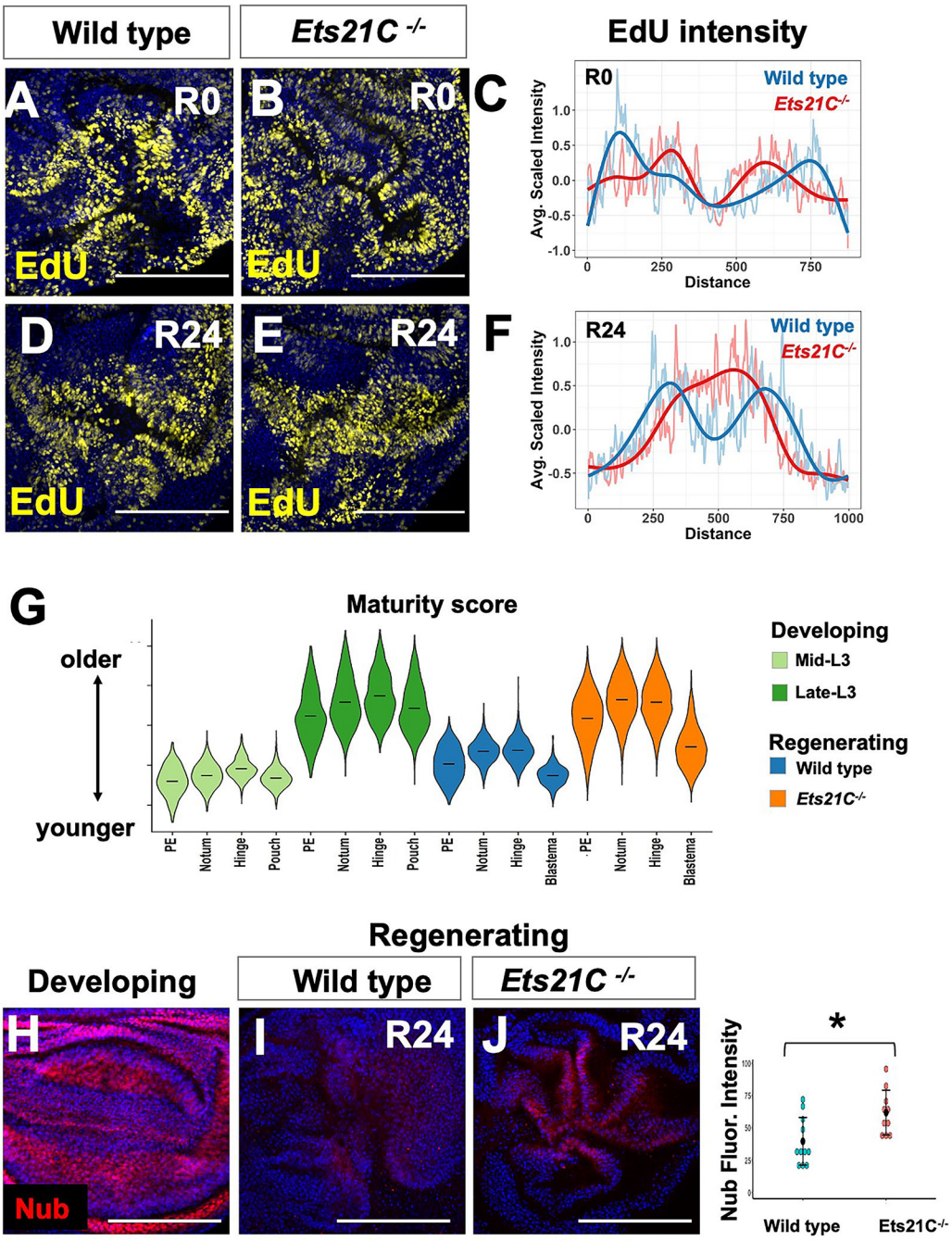

Figure 5. *Ets21C* is required to maintain a pro-regenerative program.

(**A-F**) Cell proliferation for wild type and *Ets21C*$^{-/-}$ discs as assessed by EdU incorporation at R0 and R24. (**C, F**) Profiles of average EdU intensity across the blastema at each regeneration time point (see Materials and Methods). Note that the EdU intensity decreases within the center of the blastema in both genotypes at R0 but only in wild type at R24. (**G**) Cellular maturity score for individual cells, calculated by the weighted expression of genes that distinguish mid and late developing discs in scRNAseq data (see Materials and Methods). Note that the wild type regenerating cells have a lower maturity score than

Ets21C$^{-/-}$ regenerating cells. See also Figure S5. (**H-J)** Developing and regenerating tissue stained with antibody to pouch marker (Nub). Fluorescence intensity is quantified with statistical significance calculated via t-test (*$p < 0.05$). Microscopy scale bars = 100 μm.

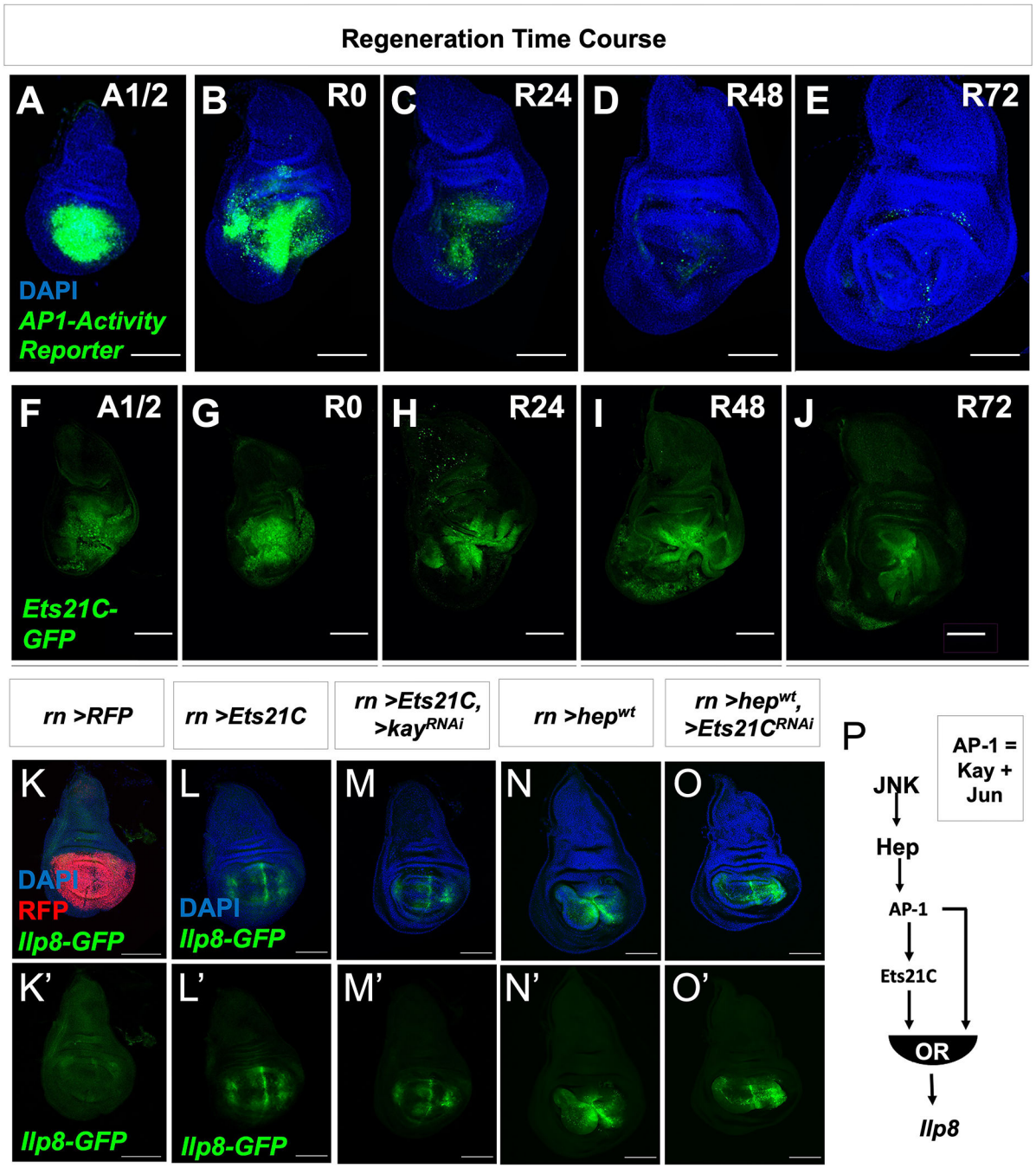

Figure 6. JNK/AP-1 and Ets21C form a feed-forward loop to sustain target gene expression.

(**A-E**) Expression of AP-1-activity reporter *(AP-1-GFP)* and (**F-J**) *Ets21C-GFP* over the course of regeneration. Wing imaginal discs were dissected half-way (20 h) through the ablation period (A1/2) and at time points after the downshift to 18°C (indicated in hours) during regeneration (R0, R24, R48, R72). Regeneration is near complete by 72 h. (**K-O**) The pouch driver *rotund (rn-GAL4)* was used to drive the overexpression of (**K**) *UAS-RFP,* (**L**) *UAS-Ets21C,* (**M**) *UAS-Ets21C* together with *UAS-kayak-RNAi* (kayak (kay) encodes for one component of the AP-1 complex), (**N**) *UAS-hep*^{wt} (upstream activating kinase of AP-1),

and (**O**) *UAS-hep*^{wt} together with *UAS-Ets21C-RNAi.* Note that all conditions besides the control (*UAS-RFP*) resulted in the expression of *Ilp8-GFP* within the pouch. (**P**) From these overexpression data, the time course of AP-1 activity and *Ets21C* expression (**A-J**), and loss-of-function experiments (Figure 4; Figure S4), we predict that JNK/AP-1 and Ets21C form a type 1 coherent feed-forward loop to control the expression of *Ilp8* with either pathway being able to activate expression independently of the other. Microscopy scale bars = 100 μm. See also Figure S6.

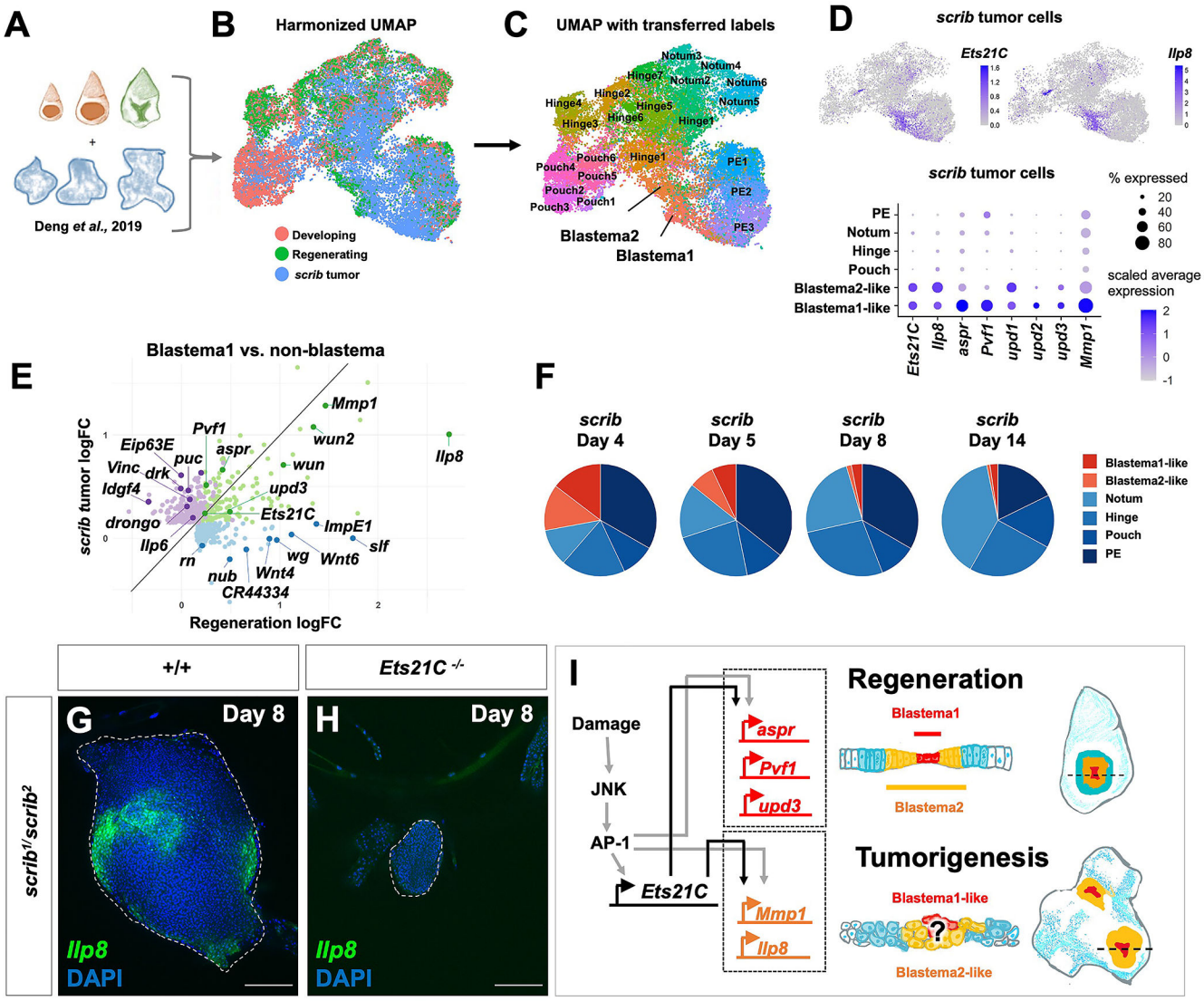

Figure 7. Blastema-like cells present in tumorigenic discs.

(**A**) Diagram of combined single-cell data. (**B**) Harmonized UMAP of epithelial cells from developing, wild-type regeneration, and *scrib* tumorigenic discs, with cells colored by sample of origin. (**C**) Harmonized UMAP colored by cell annotation as generated by transferring labels from the regeneration cell atlas. Note presence of many Blastema-like cells within *scrib* tumors. (**D**) Expression *Ets21C* and *Ilp8* in *scrib* tumor cells on UMAP and dot plot (along with other blastema markers). (**E**) Natural-log fold-change plot for differentially-expressed genes (Bonferroni p-value < 0.05) in Blastema1 cells vs non-blastema cells within wild-type regeneration data (blue dots), *scrib* data (purple dots), or both datasets (green dots). (**F**) Cell composition (based on transferred labels) within the *scrib* datasets over tumor time course. (**G-H**) *scrib*$^{-/-}$ mutant tumor with *Ilp8-GFP* in wild type and *Ets21C*$^{-/-}$ mutant backgrounds. (**I**) Proposed model of GRN downstream of Ets21C during regeneration and tumorigenesis. Microscopy scale bars = 100 μm.

Key resources table

REAGENT or RESOURCE	SOURCE	IDENTIFIER
Antibodies		
mouse anti-Wg (4D4)	Developmental Studies Hybridoma Bank	RRID: AB_528512
mouse anti-dMMP1 (14A3D2)	Developmental Studies Hybridoma Bank	RRID: AB_579782
mouse anti-dMMP1 (3A6B4)	Developmental Studies Hybridoma Bank	RRID: AB_579780
mouse anti-dMMP1 (5H7B11)	Developmental Studies Hybridoma Bank	RRID: AB_579779
rat anti-Elav (Elav-7E8A10)	Developmental Studies Hybridoma Bank	RRID: AB_528218
mouse anti-beta-galactosidase (40-1a)	Developmental Studies Hybridoma Bank	RRID: AB_528100
mouse anti-nubbin (nub 2D4)	Developmental Studies Hybridoma Bank	RRID: AB_2722119
rat anti-Zfh2	[66]	RRID: AB_2569892
rat anti-Pvf1	[67]	RRID: AB_2569381
rabbit anti-cleaved Death Caspase-1	Cell Signaling	RRID: AB_2721060
rabbit anti-Phospho-Histone H3 (PHH3)	Millipore-Sigma	Product #: 369A-1
goat anti-rat IgG- Alexa Fluor® 647	Cell Signaling	RRID: AB_1904017
goat anti-mouse IgG- Alexa Fluor® 555	Cell Signaling	RRID: AB_1904022
goat anti-rabbit IgG- Alexa Fluor® 647	Cell Signaling	RRID: AB_10693544
goat anti-chicken IgG- Alexa Fluor® 647	Thermo Fisher	RRID: AB_2535866
Chemicals, peptides, and recombinant proteins		
DAPI	Sigma Aldrich	
Schneider's *Drosophila* Media	Thermo Fisher	Cat#21720024
Critical commercial assays		
10× Genomics v2 Chip + v3.1 Chip	10× Genomics	10xgenomics.com
HCR reagents (hairpins and buffers)	Molecular Instruments	molecularinstruments.com
HCR probes	Molecular Instruments	molecularinstruments.com
EdU Assay: Click-iT EdU Cell Proliferation Kit (C10338 and C10340)	ThermoFisher Scientific	thermofisher.com
Deposited data		
Single-cell transcriptomic data: wild-type and *Ets21C*-mutant regenerating wing discs (two replicates for each genotype)	This paper	GSE174326
Experimental models: Organisms/strains		
rn-GAL4, tub-GAL80^{ts}, UAS-egr	[7]	Bl51280
rn-GAL4, tub-GAL80^{ts}, UAS-rpr	[7]	
Ets21C$^{\Delta 10}$	[39]	

REAGENT or RESOURCE	SOURCE	IDENTIFIER
UAS-Ets21C (UAS-Ets21C-long)	[39]	
UAS-Ets21C-RNAi	[39]	
Ets21C-GFP (*Pbac-Ets21C-GFP.FLAG*^{VK00033})	Bloomington Stock Center	Bl38639
Him-GFP	[62]	
Ilp8-GFP (*Ilp8*^{MI00727})	Bloomington Stock Center	Bl33079
Df(2L)BSC456	Bloomington Stock Center	Bl24960
Df(2L)BSC107	Bloomington Stock Center	Bl8673
hh-Gal4	*P-GAL4 hhGal4*	FBti0017278
rn-Gal4	*P-Gaw rnGAL4-5*	FBti0023720
UAS-hep^{wt}	*P-w[+mC]=UAS-hep.B*	Bl9308
UAS-kay-RNAi	Bloomington Stock Center	Bl33379
UAS-JNK^{DN} *(UAS-bsk-K53R)*	Bloomington Stock Center	Bl9311
Ubi-FRT-stop-FRT-GFP^{nls}	[63]	Bl32251
3XUAS-FLP.G5.PEST	Bloomington Stock Center	Bl55809
lexAOp-FLP	Bloomington Stock Center	Bl55819
GMR26E03-lexA	[64]	Bl54354
arm-lacZ FRT40A	Bloomington Stock Center	Bl7371
FRT40A	Bloomington Stock Center	Bl1816
hsFLP; ubi-RFP, FRT40A	Bloomington Stock Center	Bl34500
Act5C-FRT-stop-FRT-GAL4	Bloomington Stock Center	Bl4780
hsFLP	Bloomington Stock Center	Bl8862
arm-lacZ FRT40A	Bloomington Stock Center	Bl7371
eyFLP	Bloomington Stock Center	Bl5580
AP-1-activity reporter (*AP-1-GFP*)	[65]	Bl59010
Act5C>FRT.CD2>GAL4, UAS-RFP	Bloomington Stock Center	BL:30558
scrib^{1}	[61]	
scrib^{2}	[57]	
UAS-his::RFP	[60]	
Software and algorithms		
scvi-tools	[21]	scvi-tools.org
scANVI	[74]	scvi-tools.org
Seurat	[75]	satijalab.org/seurat
Python	[73]	python.org
Scanpy	[76]	scanpy.readthedocs.io
UMAP	[78]	umap-learn.readthedocs.io
Image J / Fiji	[68]	fiji.sc
Slingshot	[79]	bioconductor.org/packages/release/bioc/html/slingshot.html

REAGENT or RESOURCE	SOURCE	IDENTIFIER
10× Genomics CellRanger	[71]	10xgenomics.com
Other		
Single-cell transcriptomics: Developing wing discs (two time points, two replicates)	[19]	GSE155543
Single-cell transcriptomics: *scrib* tumorous wing discs (four time points)	[22]	GSE130566
Code for single-cell analysis (in R and Python)	This paper	https://github.com/HariharanLab/Worley_Everetts_Yasutomi